Multiwavelength Observations of the Second Largest Known FR II Radio Galaxy, NVSS 2146+82

Christopher Palma[1] & Franz E. Bauer[2]
Department of Astronomy, University of Virginia

William D. Cotton & Alan H. Bridle
National Radio Astronomy Observatory[3]

Steven R. Majewski[4] & Craig L. Sarazin
Department of Astronomy, University of Virginia

ABSTRACT

We present multi-frequency VLA, multicolor CCD imaging, optical spectroscopy, and *ROSAT* HRI observations of the giant FR II radio galaxy NVSS 2146+82. This galaxy, which was discovered by the NRAO VLA Sky Survey (NVSS), has an angular extent of nearly $20'$ from lobe to lobe. The radio structure is normal for an FR II source except for its large size and regions in the lobes with unusually flat radio spectra. Our spectroscopy indicates that the optical counterpart of the radio core is at a redshift of $z = 0.145$, so the linear size of the radio structure is $\sim 4 h_{50}^{-1}$ Mpc, $H_0 = 50 h_{50}$. This object is therefore the second largest FR II known (3C 236 is $\sim 6 h_{50}^{-1}$ Mpc). Optical imaging of the field surrounding the host galaxy reveals an excess number of candidate galaxy cluster members above the number typically found in the field surrounding a giant radio galaxy. WIYN HYDRA spectra of a sample of the candidate cluster members reveal that six share the same redshift as NVSS 2146+82, indicating the presence of at least a "rich group" containing the FR II host galaxy. *ROSAT* HRI observations of NVSS 2146+82 place upper limits on

---

[1]NOAO WIYN Queue Investigator

[2]National Radio Astronomy Observatory Jansky Pre-Doctoral Fellow

[3]The National Radio Astronomy Observatory is a facility of the National Science Foundation operated under cooperative agreement by Associated Universities, Inc.

[4]David and Lucile Packard Foundation Fellow; Cottrell Scholar of the Research Corporation; National Science Foundation CAREER Fellow; Visiting Associate, The Observatories of the Carnegie Institution of Washington

the X-ray flux of 1.33×10^{-13} ergs cm^{-2} s^{-1} for any hot IGM and 3.52×10^{-14} ergs cm^{-2} s^{-1} for an X-ray AGN, thereby limiting any X-ray emission at the distance of the radio galaxy to that typical of a poor group or weak AGN. Several other giant radio galaxies have been found in regions with overdensities of nearby galaxies, and a separate study has shown that groups containing FR IIs are underluminous in X-rays compared to groups without radio sources. We speculate that the presence of the host galaxy in an optically rich group of galaxies that is underluminous in X-rays may be related to the giant radio galaxy phenomenon.

Subject headings: galaxies: distances and redshifts — galaxies: individual: (NVSS 2146+82) — galaxies: photometry — radio continuum: galaxies — X-rays: galaxies

1. Introduction

The "giant" radio galaxies (GRGs), which we define as double radio sources whose overall projected linear extents exceed $2h_{50}^{-1}$ Mpc, are interesting as extreme examples of radio source development and evolution. Members of this class, which comprise only a few percent of all powerful extragalactic radio sources, have been documented for almost 25 years (e.g., Willis, Strom, & Wilson 1974). They have been used to constrain the spectral aging and evolution of radio sources and as tests for the evolution of conditions in intergalactic environments on Mpc scales (Strom & Willis 1980; Subrahmanyan & Saripalli 1993; Cotter, Rawlings, & Saunders 1996). Their 1.4 GHz radio powers are generally in the regime $10^{24.5} < P_{1.4} < 10^{26}\ h_{50}^{-2}$ W Hz^{-1}, just above the transition between Fanaroff-Riley Types I (plumed) and II (lobed) radio structures (Fanaroff & Riley 1974). It is unclear whether the giant sources are examples of unusually long-lived (and directionally stable) nuclear activity in radio-loud systems, or of the development of sources in unusually low-density environments.

Because of their large angular sizes, nearby giant radio galaxies can in principle be studied in great detail, but their largest-scale structures may be over-resolved and undersampled by interferometers. They have traditionally been discovered through sky surveys with compact interferometers or single dishes at relatively low frequencies, where angular resolution is modest but large fields of view and diffuse steep-spectrum structures can be imaged more easily. The source NVSS 2146+82 was noted as a candidate giant radio galaxy when it appeared in the first 4° by 4° field surveyed by the NRAO VLA Sky Survey

(NVSS: Condon et al. 1998), a northern-hemisphere survey at 1.4 GHz using the VLA D configuration at 45″ (FWHM) resolution.

Figure 1 shows contours of the NVSS image at 45″ resolution. There are two symmetric, extended lobes (D and E) on either side of an unresolved component C, plus an unusually large number of other radio sources within 10′ of C. Two of these (A and B) are also symmetrically located around C.

Comparison with the Digital Sky Survey (DSS) showed that source C coincides with an $\sim 18^{\rm th}$ mag elliptical galaxy to within the uncertainties in the NVSS and DSS positions. If the elliptical galaxy is the host of an unusually large radio source (C+D+E), then the apparent magnitude suggests that the whole structure may be similar in linear scale to 3C 236. The DSS also shows a nearby image that might be another galactic nucleus, and a faint extended feature suggesting a possible "tail" or interaction.

We have undertaken several observational studies of the radio and optical objects in the field to determine their nature and to clarify the relationships between the optical and radio sources. These studies include:

1. High resolution radio imaging at 4.9 and 8.4 GHz to locate any compact flat-spectrum radio components in the field, and thus to identify any AGN that could be responsible for some or all of the other radio emission,

2. A search for fainter diffuse radio emission between the D and E components that might link them together or to other sources in the field and thus clarify their physical relationship,

3. Higher-resolution radio imaging of the other radio sources in the field to explore whether they might be physically related to the diffuse components, or to each other by gravitational lensing,

4. Optical spectroscopy of both optical "nuclei" and other galaxies in the field,

5. UBVRI optical photometry of the field, and

6. X-ray imaging using *ROSAT* HRI observations to search for any hot X-ray emitting gas which might be associated with an overdensity of galaxies or non-thermal X-ray emission from an AGN.

Throughout this paper, we assume a Hubble constant $H_0 = 50h_{50}$ km s^{-1} Mpc^{-1} . At a redshift of $z = 0.145$, the angular diameter distance to the radio galaxy is $708.4h_{50}^{-1}$ Mpc, the luminosity distance is $928.7h_{50}^{-1}$ Mpc, and 1′ corresponds to $206h_{50}^{-1}$ kpc.

2. Radio Observations

Table 1 gives a journal of our VLA observations. The observations in the A configuration were designed to locate any compact radio components in the field. Those in the B, C, and D configurations were intended to image the largest scale emission in enough detail to reveal any relationships and connections between the extended components, as well as to determine their spectral and Faraday rotation/depolarization properties. The BnC configuration data were designed as a sensitive search for connections, such as jets, between the central radio source and the extended features.

The flux density calibration was based on 3C 48 and 3C 286. The on-axis instrumental polarization corrections were determined from observations of the unresolved synthesis phase calibrator 2005+778, and the absolute polarization position angle scale from observations of 3C 286. Multiple observations of 3C 286 and other polarized sources were used to detect problems with ionospheric Faraday rotation, but none was noted in any of the sessions. The data were calibrated using the source 2005+778 as an intermediate phase reference, then self-calibrated using AIPS software developed by W. D. Cotton for the NVSS survey.

Due to the large size of this source, 1.4 and 1.6 GHz observations used three pointings; one on the central source C, and one near the center of each putative lobe. The B, C, and D VLA configuration observations were made at 1.365 and 1.636 GHz to measure rotation measure and spectral index. The data from these frequencies were calibrated and imaged separately. Data taken in the BnC configuration were in two adjacent 50 MHz bands centered on 1.4 GHz. Since the source extent is comparable to that of the antenna pattern and the bandwidth used was relatively large, the deconvolution (CLEAN) and self calibration applied corrections for the frequency dependence of the antenna pattern. Data from each of the three pointings were imaged independently and combined into a single image by interpolating the images onto a common grid, averaging weightings by the square of the antenna power pattern, and correcting for the effects of the antenna pattern. The 0.3 GHz observations were of limited use owing to interference.

2.1. Radio Results

The most sensitive image of NVSS 2146+82 is derived from our BnC configuration data at 1.4 GHz which has a resolution of $13''$ (FWHM). Figure 2 shows logarithmic contours of the total intensity in the region around the source in this image; the rms noise is 20 μJy per CLEAN beam area. A gray scale representation of the same image showing the filamentary structure of the lobes is given in Figure 3. Figure 4 shows the inner region of this image

contoured to lower levels using an initially linear contour interval.

2.2. Association of Features

The structures of the extended features D and E shown in Figures 2 and 3 are entirely consistent with their being associated with each other as the two lobes of a large FR II double source of overall angular size 19.′5. Both features are brightest in the regions furthest from C, contain bright (but resolved) substructure near their outer edges resembling the hot spots of FR II sources, and have their steepest brightness gradients on their outer edges. The overall length of the two lobes is the same to within 5%. Although features A and B in Figure 1 appear symmetric around feature C, the higher resolution VLA images (Figures 2 and 3) reveal them to be background sources, unrelated to NVSS 2146+82.

The northern feature (D) contains a region of enhanced emission (hot spot) at its northern extremity with about 65 mJy in an area 30″ by 18″ and an L-shaped extension to the West. The southern feature (E) has 75 mJy in a region of enhanced emission 50″ by 30″ (a "warm spot") recessed by 10% of the distance from the core and sharp brightness gradients around its southern and western boundaries. Both regions of enhanced emission show evidence of finer, but resolved, structure in our data taken in the B configuration (see contour plots in Figure 5). Figure 3 clearly shows that the internal brightness distributions of both lobes are non-uniform, and suggest the presence of filamentary structures, again a common characteristic of FR II radio lobes at this relative resolution.

Most importantly, Figures 2, 3, and 4 also show that these lobes are linked to the central compact feature C by elongated features that are plausibly the brightest segments of a weak jet-counterjet system. These features are labeled in Figure 4.

We interpret the following features as belonging to the jet in the south lobe.

J1. This feature is clearly part of a jet that points towards the south lobe but not directly at the peak of feature E.

J2. This feature (1.′5 from C) and feature K (1.′4 to the north of C) are roughly symmetric in distance from C and in intensity but are not quite collinear with C. On both sides of the source the jet becomes harder to trace further into the lobe. J2 appears to be south of the C–J1 direction, suggesting a southward bend, however.

J3. This feature is plausibly a knot in the continuation of the jet into the south lobe. The lobe brightens beyond J3 and contains a diffuse ridge that is a plausible continuation of the (possibly decollimated) jet in the direction of the "warm spot" E. The north lobe also

brightens at about the same distance from C although there is no feature corresponding to J3 in the north.

Table 2 gives flux density estimates for the main features of the source. We estimate that the jet and counterjet together comprise about 1% of the total flux density of the extended lobes, a typical jet "prominence" for radio galaxies slightly above the FR I–II transition.

The higher-resolution radio images provide no evidence that sources A, B, or F in Figure 1 are physically related to each other, or to C, D and E. Although none can be optically identified, we consider it likely that these are three (or more) unrelated background sources. The symmetrical alignment of A and B around C is apparently coincidental, and there is no evidence for any radio "bridge" between these sources and component C.

2.3. Polarimetry

The polarization structure derived from the sensitive BnC configuration observations is shown in Figure 6. The 1.4 and 1.6 GHz data are sufficiently separated in frequency to enable us to measure Faraday rotation but still maintain comparable surface brightness sensitivity. The derived rotation measure images of the two lobes are shown in Figure 7. The rotation measure distribution over the north lobe is featureless but several filamentary rotation measure structures can be seen over the southern lobe. The average rotation measure is about the same in the two lobes, -9 rad m^{-2} in the north and -8 rad m^{-2} in the south. The Faraday rotation measure in the south lobe has a somewhat larger root mean square variation, 8 rad m^{-2} compared to 5 rad m^{-2} in the north.

2.4. Spectral Index Distribution

Figure 8 shows the 0.35 to 1.4 GHz spectral index distribution inferred from comparing the WENSS (Rengelink et al. 1997) image with our BnC configuration image convolved to the same resolution. The northern and southern warm spots have spectral indices[5] $\alpha_{0.35}^{1.4}$ of -0.6 and -0.55, not unusual for the hot spots of FR II sources in this frequency regime. The background sources also exhibit spectral indices that are quite typical of extragalactic sources (A, -0.68; B, -1.0; F, -0.7). Near the centers of the north and south lobes of NVSS 2146+82, however, this comparison shows regions of unusually "flat" spectral index

[5]Spectral index, α, as used here is given by $S = S_0\nu^{\alpha}$.

($\alpha_{0.35}^{1.4} \approx -0.3 \pm 0.02$ in the north lobe, $\alpha_{0.35}^{1.4} \approx -0.4 \pm 0.03$ in the south lobe).

The spectral index variations across the lobes can also be studied from our 1.36 and 1.63 GHz data. Due to the low surface brightness the data were tapered to 55″ resolution before imaging for this comparison. To eliminate any complication from the mosaicing technique, only data derived from the pointing on a given lobe were used to determine the spectral index variations for that lobe. Thus, the data from two pointings were imaged independently at 1.36 and 1.63 GHz, corrected for the antenna power pattern, and spectral index images were derived independently for the two lobes. These results are shown in Figure 9. The close spacing of the frequencies makes determining the spectral index more difficult; but this is compensated to some extent by the nearly identical imaging properties at the two frequencies, which reduce systematic errors. These data sets are fully independent of those used for the spectral index image in Figure 8, but also reveal symmetric regions of unusually flat spectral index, $\alpha_{1.4}^{1.6} \approx$ -0.3±0.08, in both lobes.

We conclude that four independent data sets show evidence for regions with $\alpha_{0.35}^{1.4} \approx$ -0.3 in regions of relatively high signal to noise ratio. These regions are not artifacts of "lumpiness" in the zero levels of the images.

2.5. Source Alignment

NVSS 2146+82 is not aligned along a single axis. The two warm regions (E and D) and the core (C) are not collinear. The jet in the south appears to have several bends; one near the end of J1 (see Figure 4) where it bends toward J2, a change in position angle from -150° to -170°. Beyond J3, the ridge line of the lobe is fairly well defined and is again at position angle -150°, consistent with a second bend (apparently ≈ 20°) in the neighborhood of J3. The jet is not so prominent in the north but feature K, which may be the brightest part of a counterjet, is elongated along position angle of -169°.

The general "C" shape of the source suggests that the overall misalignment is due to environmental effects that have bent the jets, rather than to a changing initial jet direction which is likely to produce overall "S" symmetry.

We consider it beyond doubt that C, D and E comprise a single large FR II radio source with weak radio jets, whose parent object is the galaxy identified with C.

3. Optical Observations of NVSS 2146+82 and its Environs

Optical photometric and spectroscopic observations were obtained to identify the host galaxy of the radio emission and to measure its redshift. We began the search for the optical counterpart to the radio source using the Digitized Sky Survey (Lasker et al. 1990; hereafter DSS). The radio core is aligned with an elliptical galaxy on the DSS image to within the astrometric accuracy of the radio and optical positions from the NVSS and DSS. There is also a second, equally bright object a few arcseconds east of the galaxy at the radio core position. Finally, in the DSS image, there appears to be S–shaped diffuse emission that passes through both bright "nuclei". Therefore, our initial assumption was that the host galaxy of NVSS 2146+82 was possibly a disturbed, double nucleus galaxy. In the following sections, we summarize the optical imaging of the field surrounding the candidate host galaxy and the spectroscopic observations of this host galaxy and its candidate galactic companions.

3.1. Photometric Observations

U, B, V, R, and I CCD observations were obtained at the 1.52-m telescope at Palomar Observatory on the nights of 7-9 January 1997. In addition, U, B, V, and I CCD observations were made at Kitt Peak National Observatory on 4 April 1997. The Palomar 1.52-m observations were made with a 2048 × 2048 CCD with a pixel scale of $0\farcs37$ per pixel, resulting in a $12\farcm63$ field of view. Though photometric, the seeing was poor ($2-5''$ on 7 January, $1.5-2.5''$ on 8,9 January) during the Palomar run, so higher resolution ($1.2-1.4''$ seeing) images were obtained with the KPNO 4-m telescope in April. The KPNO observations were made with the prime focus T2KB CCD with a pixel scale of $0\farcs47$ per pixel, resulting in a $16'$ field of view. Because the KPNO data were not taken in photometric conditions, the Palomar data remained useful for calibration. Data from both observing runs were reduced using the standard IRAF CCDRED reduction tasks.

After the initial reduction, aperture photometry was performed on the host galaxy of NVSS 2146+82 using the IRAF package APPHOT. Unfortunately, due to the poor seeing on the first night of the Palomar run and the proximity of the foreground star (see §3.3) to the AGN host, it was impossible to photometer NVSS 2146+82 without significant flux contamination from the foreground star. Therefore, we used the DAOPHOT II package (Stetson 1987) to PSF fit and subtract stars from the Palomar NVSS 2146+82 images.

After the foreground star was subtracted, photometry of the galaxy was performed identically to the photometry of several Landolt (1992) standard stars. Approximately 20

stars were selected from each frame containing the AGN host galaxy. A circular aperture 2.5 times the average FWHM of these stars was used to measure the flux of the host galaxy. This aperture was chosen to be consistent with the standard star photometry and because it completely enclosed the host without including contaminating flux from other nearby objects.

Once instrumental magnitudes for the galaxy were determined, they were transformed to the standard system using transformation equations incorporating an airmass and color term that were determined for the Landolt standard stars. The results of our U,B,V,R,& I photometry of the host galaxy are listed in Table 3.

3.2. Spectroscopic Observations

Optical spectra of NVSS 2146+82 were obtained at Kitt Peak National Observatory on 9 December 1996. The spectroscopic observations were made with the RC Spectrograph on the KPNO Mayall 4-meter telescope. The detector in use was the T2KB CCD in a 700 $\times$ 2048 pixel format. All exposures were made with a $1''$ slit width and a 527 lines/mm grating. The spectral resolution, measured using unresolved night sky lines, is $\sim$3.4 Å. The data were reduced using the standard IRAF reduction tasks. The extracted spectra were wavelength calibrated using a solution determined from the spectrum of a HeNeAr comparison source. Finally, spectrophotometric calibration was applied using a flux scale extrapolated from several standard star spectra.

Spectra of candidate galactic companions to NVSS 2146+82 (see §3.5 below) were obtained with the HYDRA multi-fiber positioner and the Bench Spectrograph as part of the WIYN[6] Queue Experiment over the period of 14-22 September 1998. The T2KC CCD was used as the spectrograph detector in its spatially binned 1024 $\times$ 2048 pixel mode. All exposures were made with the red fibers, the Simmons camera, and a 400 lines/mm grating. The spectral resolution in this configuration is $\sim$4.5 Å.

We calculated an astrometric solution for the KPNO 4-m frame of the NVSS 2146+82 field using positions for stars in the frame taken from the USNO A1.0 catalog (Monet et al. 1996). Using this solution, we derived positions with the accuracy required by the HYDRA positioner for our target galaxies. Due to fiber placement restrictions and the density of our target galaxies on the sky, we were only able to place 46 fibers on targets. The remaining 50

[6]The WIYN Observatory is a joint facility of the University of Wisconsin-Madison, Indiana University, Yale University, and the National Optical Astronomy Observatories.

fibers were randomly placed on blank sky, and they were used during the reduction process for night sky subtraction.

The nine 30 minute program exposures were reduced using the IRAF DOHYDRA script. The weather conditions during the last two nights were poor, and the spectra from these nights were not usable. Therefore the final spectra were obtained by co-adding only the data from nights one and two, a total of two hours of integration.

3.3. Redshifts and Line Luminosities

In Figure 10, we present a contour plot of the V band surface brightness from the central $40'' \times 40''$ region of the KPNO 4-m image after smoothing with a 3 pixel by 3 pixel boxcar kernel. Although we find that the elliptical galaxy at the radio core position ($\alpha = 21^{\rm h}45^{\rm m}30^{\rm s}$, $\delta = +81^\circ 54' 55''$ J2000.0) has a narrow line AGN emission spectrum with a redshift of $z = 0.145$, we find that the object just to the east, which was assumed to be potentially a second nucleus, has a zero-redshift stellar spectrum, indicating it is a foreground star. Figure 11 shows two plots of the wavelength and flux calibrated spectrum of the host galaxy of NVSS 2146+82.

An unusual feature of the spectrum (Figure 11) of the AGN is that all of the emission lines appear to be double peaked. The second panel in Figure 11 shows an expanded view of the [OIII] doublet clearly showing the double peaked profile of the emission lines. Each emission line was easily fit with a blend of two gaussians, indicating that AGN line emission is coming from two sources with a velocity separation of $\sim$450 km s^{-1}.

Since the AGN emission line spectrum gives two different velocities, we have decided to take the velocity of the stellar component of the galaxy as the systemic velocity of the galaxy. The stellar absorption line redshift, calculated by cross-correlating the host galaxy spectrum with the spectrum of the star immediately to the east, is 0.1450 ± 0.0002.

Table 4 lists the properties of the observed emission features in the spectrum of NVSS 2146+82. The redshifts of the AGN emission line components were calculated by identifying features and taking the average redshift of all of the identified features. In this way, the two AGN emission line components have been measured to be at velocities of 40070 ± 50 km s^{-1} and 40520 ± 50 km s^{-1}, which corresponds to redshifts of 0.1440 ± 0.0002 and 0.1456 ± 0.0002 respectively. This indicates that the gas which is giving rise to the bluer component of the AGN emission line spectrum is moving relative to the stars in the AGN host galaxy at -280 km s^{-1} and the gas emitting the redder lines is moving at 170 km s^{-1} with respect to the stars.

Each emission feature identified in Table 4 was fit with a blend of two gaussian components (except for the two weak lines [Ne III] λ3967 and [O III] λ4363, where a single gaussian was used) to determine the line flux. The fluxes listed in Table 4 were measured after the spectrum of NVSS 2146+82 was flux calibrated using the average of four measurements of the calibrator Feige 34. The flux of the calibrator varied significantly among our four separate exposures, and we therefore estimate our spectrophotometry is only accurate to about 20%. In addition to calibration error, there is an additional error in the profile fitting, and therefore the errors listed for the fluxes include both calibration and measurement error.

We derived an extinction of $A_V = 0.9 \pm 0.9$ (the large error is due mostly to the calibration error in the fluxes) using the standard Balmer line ratios for Case B recombination (Osterbrock 1989) and the extinction law of Cardelli et al. (1989). The Galactic extinction at the position of NVSS 2146+82 is given as $A_V = 0.5$ on the reddening maps of Schlegel et al. (1998). This value is consistent with our Balmer line derived value, but possibly indicates that there may be some dust in the host galaxy itself. We decided to correct the measured line fluxes for reddening using the mean value we derived of $A_V = 0.9$. The errors listed in Table 4 for the fluxes do not include the error in the extinction determination.

3.4. Optical Properties of the Host Galaxy

Sandage (1972) found that the optical luminosity function of radio galaxy hosts was similar to that of first ranked cluster members, and he noted that their optical morphology was similar to bright E galaxies. Although it was therefore generally believed that the hosts of all radio galaxies were gE types, subsequent large surveys of radio galaxies showed a good deal of evidence for peculiar morphologies (e.g., Heckman et al. 1986). We find that the host galaxy of NVSS 2146+82 is likely typical, i.e. it is a gE galaxy, but with evidence of some peculiar morphological features.

The broadband colors of NVSS 2146+82 are typical of bright FR II host galaxies. The absolute magnitude we derive for the host is $M_V = -22.9$ at $z = 0.145$ if we adopt a K correction of 0.46 magnitudes in the V passband (Kinney et al. 1996). This magnitude is consistent with the host being a gE galaxy, and also is very similar to the mean V magnitude for 50 low redshift FR IIs of -22.6 (Zirbel 1996).

Similar to other FR II host galaxies, we find the optical morphology of the host elliptical of NVSS 2146+82 to be disturbed. In Figure 10, the four distinct objects besides

the host galaxy and foreground star have been identified as having non-stellar morphologies with the Faint Object Classification and Analysis System (FOCAS, Valdes 1982). If these four galaxies share the same redshift as the gE host of NVSS 2146+82, they all lie 50–100 kpc away from its nucleus, a distance that implies that they may be dynamically interacting with it. Figure 10 also shows what appears to be a bridge of diffuse optical light that almost connects NVSS 2146+82 to the galaxy to the southwest. This bridge may indicate that this smaller galaxy has recently passed close enough to NVSS 2146+82 to interact with it gravitationally. There is also a fifth object $5''$ to the southeast of the center of NVSS 2146+82, which could be in the process of merging with the gE galaxy. However, due to the faintness of this object and its proximity to the nucleus of 2146+82, we are unable to classify this object definitively as a galaxy with the FOCAS software. Although we cannot conclude based on this image that NVSS 2146+82 is undergoing a merger, its outer isophotes do show evidence that it has been disturbed.

Correlations between the radio power and optical emission line luminosities in radio galaxies have been established in several studies (e.g., Rawlings & Saunders 1991; Zirbel & Baum 1995; Tadhunter et al. 1998). These radio/optical correlations are assumed to arise primarily due to the fact that both the radio jet and the ionization source originate in the central engine. The radio core power at 5 GHz ($\log P[W/Hz] = 23.85$) and the Hα + [N II] luminosity ($\log L[W] = 35.2$) for NVSS 2146+82 lie well within the dispersion in the correlation in these quantities found for low redshift FR IIs (Zirbel & Baum 1995). This apparently indicates that the physical conditions that cause this radio/optical correlation to arise may be similar in this GRG and in "normal" FR IIs.

The shape of the emission line profiles in NVSS 2146+82 are not unique; emission line profiles and narrow band imaging of Seyfert galaxies and radio galaxies have shown evidence for interaction between the radio synchrotron emitting plasma and the optically emitting ionized gas (see e.g., Whittle 1989). Although the majority of objects that show kinematic evidence for interactions between the radio jets and ionized gas clouds tend to have more compact radio structures, the double peaked line profiles seen in NVSS 2146+82 appear similar to those seen in radio galaxies with jet/cloud interactions. A recent model (Taylor, Dyson, & Axon 1992) for interactions between the nuclear radio emission and NLR gas in Seyferts produces [O III] profiles for objects near the plane of the sky that are very similar to the double peaked profiles seen in NVSS 2146+82. The model of Taylor et al. (1992) produces double peaks in the line profiles of objects oriented close to the plane of the sky because the emission lines are postulated to arise from gas that is being accelerated as a bowshock expands into the ionized medium surrounding the nucleus. They model the bowshock as a series of annuli, and each annulus contributes most of its luminosity at the two extreme radial velocities found along the line of sight. Although the specifics of the

model of Taylor et al. (1992), such as the discrete plasmon emission from the radio nucleus, may not necessarily apply in the case of NVSS 2146+82, it suggests that the narrow line profiles observed for this FR II (which is assumed to be very near the plane of the sky) can be produced plausibly in a model where the ionized gas is in a cylindrical geometry around the radio jet.

Double peaked *broad* lines have been observed in radio galaxies (e.g., Pictor A [Halpern & Eracleous 1994]), however the model that is typically invoked to explain the broad line profiles requires the radio galaxy to be oriented close to the line of sight. Since NVSS 2146+82 does not show a broad line component and is unlikely to be oriented close to the line of sight, the accretion disk model relied on to fit double peaked broad lines in AGN is probably unrelated to the emission line profiles observed in NVSS 2146+82.

Although a jet/cloud interaction appears to be the most reasonable explanation for the double peaked narrow emission lines observed in the spectrum of NVSS 2146+82, it is also plausible that a gravitational interaction between the FR II host galaxy and its nearest companions may be the source of the $\sim$450 km/sec separation between the blue and red emission line peaks. Higher spatial resolution long slit spectroscopy is necessary to determine which cause is more likely.

3.5. Environment

Deep CCD imaging of the region surrounding the host galaxy of NVSS 2146+82 has revealed a large number of nearby galaxies. These galaxies are near the limiting magnitude of the POSS/DSS images, so NVSS 2146+82 appears to lie in a sparsely populated region of the sky in the DSS. However, photometry from the deeper Palomar 1.52-m images gives $-22 \lesssim M_V \lesssim -19.5$ for these nearby galaxies if they also lie at $z = 0.145$, indicating a possible association with NVSS 2146+82. In Figure 12, we present a region of the KPNO 4-m image of NVSS 2146+82 that is 0.5 Mpc on a side and that has all identified galaxies with $m_v \lesssim 21.3$ (corresponding to $M_V \lesssim -19$ at $z = 0.145$) circled. These images do not go deep enough to allow accurate identification and photometry of all galaxies to $M_V = -19$, so this sample is not complete. However, even though the sample shown in Figure 12 is probably only complete to $M_V \sim -20.5$, we have identified 34 candidate galaxies surrounding NVSS 2146+82.

Although there are no previous identifications of the cluster around NVSS 2146+82 (at $b = 21\overset{\circ}{.}5$, it is too close to the Galactic Plane to have been included in the Abell [1958] catalog), there is a Zwicky cluster to the north, with NVSS 2146+82 lying only $\sim 5'$ south

of the southern border of the Zwicky cluster. The Zwicky cluster 2147.0+8155 (B1950.0 coordinates) is a compact group with 56 members classified as "extremely distant" or $z > 0.22$ (Zwicky et al. 1961). While this gives a redshift for the Zwicky cluster larger than that of NVSS 2146+82, it is close enough to $z = 0.145$ (< 400 Mpc more distant) that we may be seeing NVSS 2146+82 in projection against a background rich cluster.

In September of 1998 WIYN/HYDRA spectra were obtained of 46 candidate galactic companions of NVSS 2146+82 to determine their redshifts. The sample of 46 was selected in the following way: (1) We selected all objects morphologically classified as galaxies in the KPNO 4-m frame by FOCAS with aperture magnitudes < 21, resulting in an initial sample of 205 galaxies. (2) We divided this group into two subdivisions: the first being all galaxies within 0.5 Mpc of 2146+82 in projected radius, and the second being all those outside of the 0.5 Mpc radius. However, due to exposure time limitations, the available sample taken from the 34 galaxies identified in Figure 12 within 0.5 Mpc of the host was reduced to the 17 brightest galaxies. Fiber placement restrictions allowed us to observe only 11 of these 17 galaxies. Objects from the sample outside of the 0.5 Mpc radius from NVSS 2146+82 were assigned to 35 of the remaining fibers, leaving about 45 fibers on blank sky to allow accurate sky subtraction. Unfortunately, as mentioned in §3.2 above, the weather conditions during some of the queue observing were poor, and this limited the success of the program. There was enough signal-to-noise to identify features in the spectra of only 24 of the 46 objects successfully. We found that 7 of the 24 objects with good spectra were actually misidentified stars.

Nonetheless, from the remaining 17 spectra of galaxies in the field surrounding NVSS 2146+82, we were successful in identifying what we believe to be a true cluster that contains the radio source host galaxy. Figure 13 presents an image with the 17 galaxies with measured redshifts marked. The positions, redshifts, and magnitudes for these objects are listed in Table 5. A quality factor is assigned for each redshift using the 0 (unreliable) to 6 (highly reliable) scale of Munn et al. (1997). The quality is determined using: $q = \min[6, \min(1, N_{def}), +2N_{def} + N_{prob}]$, where N_{def} is the number of spectral features that are accurately identified (less than 5% chance of being incorrect) and N_{prob} is the number of spectral features that are probably correct (about a 50% chance of being correct). If $q > 3$ is adopted as the requirement for a reliable redshift, 5 of the 17 galaxies have unreliable redshifts. The histogram plotted in Figure 14 is a redshift distribution for the 17 galaxies, and it shows that 50% (6) of the reliable redshifts fall in the range of $z = 0.135 - 0.148$, with 5 of those having redshifts of $z = 0.144 - 0.148$.

Extrapolating the redshift distribution for the sample of galaxies identified around NVSS 2146+82 from the redshift distribution of the 17 reliable galaxy spectra suggests that

the 2146+82 cluster may be Abell richness class 0 or 1. Of course, the statistics are very uncertain. Of the 11 galaxies within a projected distance of 0.5 Mpc of NVSS 2146+82 that were in the WIYN/HYDRA sample, redshifts were measured for three of them. Two of these have $z = 0.144 - 0.145$, while the third has $z = 0.135$. We identified features in 21 of the remaining 35 spectra that were measured for objects outside of the projected 0.5 Mpc radius. We found that 7 were misclassified stars, and 3 of the 14 galaxies with reliable redshifts had $0.144 < z < 0.148$. Abell's (1958) richness criterion was based on the number of cluster galaxies within the range m_3 to $m_3 + 2$ (m_3 is the magnitude of the third brightest cluster member). For the NVSS 2146+82 cluster, m_3 should be < 18.3, since the third brightest galaxy of the 7 (which includes NVSS 2146+82) we have found at $z = 0.145$ has $m = 18.3$. Of the 205 galaxies originally found in the KPNO 4-m field containing NVSS 2146+82, 123 of these fall within the m_3 to $m_3 + 2$ range used for estimating the Abell richness. If we apply the percentages above to this sample of 123 galaxies, then 37 ± 13 might be at the same redshift as NVSS 2146+82. To this point, we have been considering the cluster richness inside of 0.5 Mpc, for comparison with the $N_{0.5}^{-19}$ richnesses of Allington-Smith et al. (1993) and Zirbel (1997), and also within an area ∼3.8 Mpc on a side, which is the size of the KPNO 4-m field at $z = 0.145$. However, we must note that the original richness criterion for Abell class 1 clusters was that 50 or more galaxies were contained in a radius of 3 Mpc for $H_0 = 50$ km sec^{-1} Mpc^{-1} (Abell 1958). A circle of radius $3h_{50}^{-1}$ Mpc at $z = 0.145$ subtends 507 square arcminutes on the sky, nearly twice the amount of area covered in our image. If the calculated optical richness from the 4-m image galaxy sample is taken as a lower limit to the number of galaxies within an Abell radius, the richness class of the group surrounding NVSS 2146+82 appears to be at least Abell class 0.

4. X–ray Observations and Constraints

Richness class 0 clusters of galaxies typically have luminosities with $L_x \approx 10^{43-45}$ ergs s^{-1} (Ebeling et al. 1998), while X-ray AGN range from $L_x \approx 10^{40-44}$ ergs s^{-1} (Green, Anderson & Ward 1992), so a cluster or bright AGN will easily be seen with a medium length exposure with *ROSAT*. NVSS 2146+82 was observed with the *ROSAT* High Resolution Imager (HRI) between 1998 February 24 and 1998 March 13 for a duration of 30.3 ksec to search for any hot gas that might be associated with the apparent overdensity of galaxies or for an X-ray luminous AGN.

The data were analyzed with the IRAF Post-Reduction Off-line Software (PROS). The HRI data were filtered for periods of high background and corrected for non-X-ray background, vignetting, and exposure using the computer programs developed by Snowden

(Plucinsky et al. 1993; Snowden 1998). After filtering, the live exposure was 29.8 ksec. The resulting X-ray image was convolved with a gaussian beam with $\sigma = 2''$ to recover diffuse X-ray emission. The contours of the image are shown superposed on the DSS image in Figure 15.

A few sources were visible near the edge of the field, but there seem to be no significant sources of X-ray emission associated with any optical or radio sources within the $20'$ extent of NVSS 2146+82 (Figure 15). We derived upper limits on both the AGN or cluster emission by extracting the X-ray counts from the corrected X-ray image using circular regions centered on the host galaxy of $20''$ and $2'.25$, respectively. The region sizes were chosen simply because $20''$ represents the size of a typical HRI point source and $2'.25$ is roughly 1-2 times the typical size of a cluster core at the distance of the radio galaxy. The X-ray background was determined by extracting the X-ray counts from an annulus of $2.25 - 5'$ centered on the nucleus of the radio host and removing 3 point sources using $20''$ circular regions. We used PIMMS (Mukai 1993) to convert the HRI count rate into an unabsorbed flux in the 0.1-2.0 keV band, assuming an emission model and a Galactic photoelectric absorption column of 1.058×10^{21} cm^2 (Stark et al. 1992). For the AGN, we assumed a power law with a photon index, Γ, of 2.0 and derived an upper limit at the 90% confidence level of 3.52×10^{-14} ergs cm^{-2} s^{-1}, or $3.63 \times 10^{42}\ h_{50}^{-2}$ ergs s^{-1} at the distance of the radio galaxy. Similarly for the cluster, we assumed a Raymond-Smith thermal emission spectrum characterized by $kT = 1$ keV which yielded an upper limit of 1.33×10^{-13} ergs cm^{-2} s^{-1}, or $1.37 \times 10^{43}\ h_{50}^{-2}$ ergs s^{-1}.

Unfortunately, our limit on the X-ray emission from the radio galaxy is not very stringent. Fabbiano et al. (1984) studied the X-ray properties of several 3CR radio galaxies with the *Einstein* Observatory. They found that the FR II's radio and X-ray luminosities are strongly correlated. Thus with a radio flux of 6.8 mJy at 5 GHz, NVSS 2146+82 should have a nuclear X-ray flux of a few times 10^{42} ergs s^{-1}. This flux is comparable to our upper limit. Taking into account the intrinsic scatter in the radio/X-ray correlation, our non-detection of the AGN is quite reasonable.

Our upper limit on the X-ray emission from hot cluster gas provides a much stronger constraint. Most Abell richness class 0 clusters have X-ray luminosities of $\approx 10^{43-45}$ erg/s (Ebeling et al. 1998). Therefore any cluster of galaxies associated with the radio galaxy must be either intrinsically weak in X-rays or must be poorer than our optical estimate. Wan & Daly (1996) studied the X-ray emission of low-redshift FR II galaxies and found that poor clusters that contain FR II sources are underluminous in X-rays compared to similar clusters that do not contain FR IIs. The median X-ray luminosity for low-z clusters with FR IIs was found to be $1.3 \times 10^{42} h_{50}^{-2}$ ergs s^{-1} while it is $1.33 \times 10^{43} h_{50}^{-2}$ ergs s^{-1} for

a sample of low-z clusters without FR IIs (Wan & Daly 1996). Assuming that the group surrounding NVSS 2146+82 is similar to that of other clusters found around low-z FR IIs and is underluminous in X-rays, the optical richness estimate is probably correct.

5. Discussion

5.1. Physical Properties of the Radio Source

5.1.1. Size and Luminosity

Our observations of NVSS 2146+82 clearly show that it is an unusually large FR II radio galaxy. Its angular distance from the north lobe to the south lobe gives an unusually large extent of $\theta = 19\farcm5$. For our assumed cosmology and our measured redshift of $z = 0.145$, the linear extent of the radio structure is $4h_{50}^{-1}$ Mpc, placing it in the Giant Radio Galaxy (GRG) class, which we define as sources larger than $2h_{50}^{-1}$ Mpc. NVSS 2146+82 is therefore the second largest FR II known, surpassed only by 3C236 which is $\sim 6h_{50}^{-1}$ Mpc in extent. FR II galaxies of this size are extremely rare; a literature search by Nilsson et al. (1993) of 540 FR IIs contains only 27 objects with sizes greater than $1h_{50}^{-1}$ Mpc. Of this sample of 27 large FR IIs, only 5 are larger than $2h_{50}^{-1}$ Mpc. For comparison, the other known giant radio sources are shown in Table 6. The log radio luminosity of NVSS 2146+82 at 1.4 GHz is 25.69, in the middle of the range for giant radio sources.

It remains unclear if there are fundamental differences between GRGs and "normal" radio galaxies. The relative paucity of known GRGs may be in part due to observational selection effects in past radio surveys. An alternative reason for the rarity of giant radio galaxies may be that the physical conditions necessary for the creation of a GRG are uncommon in the universe. Although the similarity between NVSS 2146+82 and other FR IIs suggests that it is a typical FR II radio galaxy at the extreme end of the size distribution, a study of a complete sample of radio galaxies that includes GRGs will have to be made to determine if GRGs are part of a continuous distribution in size of normal radio galaxies or if there are fundamental differences between GRGs and smaller FR IIs.

5.1.2. Equipartition calculations

If the usual equipartition assumptions are made, then it is possible to estimate the magnetic field strength and pressure in the lobes. Assuming that the observed spectral index is maintained from 10 MHz to 100 GHz, that there are equal energies in the radiating

electrons and other particles, and that the filling factor is unity, the derived magnetic field is $B_{min} \approx 5 \times 10^{-6}\ h_{50}^{2/7}$ Gauss and $p_{min} \approx 3.5 \times 10^{3}\ h_{50}^{4/7}$ cm^{-3}K for the hot spots. At the midpoint of the lobes these values are $B_{min} \approx 8 \times 10^{-7}\ h_{50}^{2/7}$ Gauss and $p_{min} \approx 2.3 \times 10^{2}\ h_{50}^{4/7}$ cm^{-3}K. At this redshift, the 3 K microwave background has an equivalent magnetic field of 4.2×10^{-6} Gauss so the energy loss in the lobes should be dominated by inverse Compton scattering of this background, and the time for the electrons radiating at 1400 MHz to lose half of their energy will be $\approx 10^{8}\ h_{50}^{-3/7}$ years.

5.1.3. Magnetic Field and Faraday Rotation

The mean Faraday rotation of ≈ -9 rad m^{-2} shown in Figure 7 is consistent with the results of Simard-Normandin, Kronberg, & Button (1981) for other extragalactic sources seen through this region of the Galaxy ($l = 116.^\circ7, b = 21.^\circ5$). It is therefore likely that the rotation measure screen seen in Figure 7 is primarily the foreground screen of our Galaxy. The low apparent rotation measure and the smoothness of the polarization structure shown in Figure 6 suggests that the magnetic field in this source is well ordered. The field configuration is entirely typical of older extended FR II sources, with the E vectors lying approximately perpendicular to the ridge line of the radio emission in most features.

We note that the greater variance and evidence for organized structure in the Faraday rotation of the southern lobe is the opposite of what would be expected if the jet sidedness were due to Doppler favoritism and the Faraday rotating medium were local to the source. We think it more likely that the Faraday rotation structure arises along the line of sight in our Galaxy.

5.1.4. Spectral Index Variations

The spectral index variations shown in Figure 9 indicate that there are regions $2\farcm4$ back towards C from the brightest region in each lobe that have unusually flat spectra ($\alpha_{0.35}^{1.4} \approx$ -0.3), flatter even than the hot spots. The only extended synchrotron sources known with spectra this flat are a few Galactic supernova remnants (Berkhuijsen 1986).

The spectral index structure in NVSS 2146+82 is unlike the systematic steepening of the spectrum away from the hot spots that is usually interpreted as an effect of spectral aging in extended lobes. In such interpretations, electrons are presumed to be injected into a high field region in or around the hot spots, and their energy spectrum steepens with distance as they diffuse into lower field regions of the extended lobes. Clearly no such

interpretation can be made here.

These flatter spectrum regions occur in the transition zone from the featureless parts of the lobes (closer to the core) to the parts near the regions of enhanced emission that contain significant filamentary structure. The anomalous regions are near the midline of the lobes; the southern region is centered on the path of the jet and the northern region is at one end of a prominent filament (the path of the jet is uncertain). The relative symmetry of the flatter spectrum regions of the lobes suggests that they might be produced by an intrinsic property of the source, such as a variable spectral index in the injection spectrum of the relativistic electrons from the jet, rather than local environmental effects.

If the magnetic field has values near those estimated by the equipartition calculations given above, then the energy loss of the radiating electrons is dominated by inverse Compton scattering against the Cosmic Microwave Background. In the low density, low magnetic fields in these lobes, the aging effects will be slow and the history of a variable electron spectrum could be maintained along the length of the lobe.

5.1.5. Size Scales of Symmetry in the Radio Source

There are three size scales on which symmetries appear or change in the radio structure: The first is $1\farcm5 = 300h_{50}^{-1}$ kpc. The jets appear to become symmetric on this scale but are asymmetric on smaller scales. If the J2 and K components (Figure 4) are symmetric features in the jet and counterjet, any Doppler boosting from relativistic motion must have disappeared by this point in the jet. The second scale is $3\farcm2 = 640h_{50}^{-1}$ kpc. On this scale, there is a dramatic brightening of both lobes. The third scale is $6\farcm5 = 1300h_{50}^{-1}$ kpc. At this distance, the lobes become even brighter and strong filamentary structure appears. This is the distance at which regions of spectral anomaly appear in the extended emission.

The largest scale symmetries thus suggest a symmetric overall environment, apart from the slight non-collinearity (C-symmetry) of the structure. The small scale brightness asymmetries of the jet and counterjet might be attributed to Doppler boosting and dimming by relativistic motion which effectively disappears by $\sim 300h_{50}^{-1}$ kpc, i.e. on a scale more typical of a "non-giant" FR II source. We reiterate however that the small asymmetry in rotation measure dispersion (variance) between the lobes is opposite in sign to that expected on this interpretation. This asymmetry seems more likely to reflect an intrinsic asymmetry (or gradient) in the foreground magnetoionic medium.

5.2. The Optical Environment

One possibility for the origin of GRGs is that they are otherwise normal FR II sources that reside in extremely low density gaseous environments. The environments in which radio galaxies reside have been studied in depth (e.g. Longair & Seldner 1979; Heckman et al. 1986; Prestage & Peacock 1988; Hill & Lilly 1991; Allington-Smith et al. 1993; Zirbel 1997) because the gas density and pressure in the host galaxy's ISM, any intracluster medium, and the IGM are at least partly responsible for determining the resulting radio morphology.

An intriguing result of recent studies (Hill & Lilly 1991; Allington-Smith et al. 1993, Zirbel 1997) is that FR II galaxies are found in a range of cluster richnesses at moderate redshifts, but they are only found in poor to very poor groups at low redshift. The "richness" of the cluster associated with a radio galaxy can be estimated in a statistical sense in the absence of redshift data on nearby galaxies. Allington-Smith et al. (1993) define the richness parameter $N_{0.5}^{-19}$ as the number of galaxies within a projected radius of 500 kpc and with $M_V \leq -19.0$ assuming the same redshift as the AGN. The number counts are corrected for contamination by foreground and background galaxies by subtracting number counts from a field offset from the radio galaxy. Zirbel (1997) gives a conversion of $N_{0.5}^{-19}$ to Abell class as $N_{Abell} = 2.7(N_{0.5}^{-19})^{0.9}$. With this conversion, the thresholds for Abell Classes 0 and 1 are $N_{0.5}^{-19} = 15$ and 26 respectively. Using this richness estimation technique, Zirbel (1997) found that of a sample of 29 low redshift ($z < 0.2$) FR IIs: (1) 41% of the sample of low z FR IIs reside in very poor groups ($N_{0.5}^{-19} < 3.5$), and (2) more importantly, no low redshift FR II was found in a rich group with $N_{0.5}^{-19} > 20$. Based on the results given in §3.5, NVSS 2146+82 appears to reside in a group with an anomalously high galaxy richness compared to other low redshift FR IIs. Although the galaxy counts from the field surrounding NVSS 2146+82 were not calculated identically to those of Zirbel (1997), the value of $N_{0.5}^{-19}$ is likely $> 25 - 30$ for NVSS 2146+82.

The upper limit on the cluster X-ray emission is consistent with the NVSS 2146+82 group being at the low end of the X-ray luminosity distribution for poor clusters. Wan & Daly (1996) found that in a comparison of low redshift clusters with and without FR II sources, clusters that contained FR IIs were underluminous in X-rays compared to clusters without FR IIs. Although the cluster surrounding NVSS 2146+82 may be Abell Class 0, its lack of associated X-ray gas suggests that the pressure in the surrounding medium is low enough for a giant radio source to form with little disruption of the FR II jet.

Curiously, several other GRGs listed in Table 6 also appear to lie in regions with overdensities of nearby galaxies. The GRG 0503-286 appears to lie in a group of 30 or so galaxies (Saripalli et al. 1986). These companions are concentrated to the northeast of the

host galaxy of 0503-286, and may have caused the asymmetric appearance of the northern lobe of the radio structure. Overdensities of nearby galaxies are also reported for 1358+305 (Parma et al. 1996) and 8C 0821+695 (Lacy et al. 1993); however, in both cases there is no spectroscopic confirmation of the redshifts of the candidate cluster galaxies. In a recent study of the optical and X-ray environments of radio galaxies, Miller et al. (1999) find that for a sample of FR I sources, all have extended X-ray emission and overdensities of optical galaxies. However of their sample of seven FR II sources, none have overdensities of optical galaxies or extended X-ray emission except for the GRG DA240, which has no extended X-ray emission but does have a marginally significant excess of optical companions. Perhaps for at least some of the GRG population, the presence of the host galaxy in an optically rich group with little associated X-ray gas is related to the formation or evolution of the radio source?

6. Summary and Conclusions

We have presented multi-wavelength observations of the unusually large FR II radio galaxy NVSS 2146+82. The overall size of the radio source is $4h_{50}^{-1}$ Mpc, making it the second largest known FR II source. We have found the host galaxy to be similar in both luminosity and morphology to a sample of other low redshift FR II galaxies. Emission line profiles seen in the spectrum of the host galaxy are double peaked, which may indicate that the ionized gas may be being accelerated by the bipolar radio jet.

We have also found evidence for an anomalously rich group of galaxies at the same redshift as NVSS 2146+82 that has little associated X-ray emitting gas. Though unusual in having a rich environment, this source is similar to other low redshift FR IIs in clusters; the NVSS 2146+82 group is underluminous in X-rays compared to clusters of similar richness that contain no FR II. The large radio size, lack of significant Faraday rotation and non detection of X-rays all suggest that in spite of the richness of the cluster in which this galaxy resides, it has a low gas density.

There is some morphological evidence that the host galaxy of NVSS 2146+82 may be undergoing tidal interaction with one or more of its nearest companions. Also, an interaction may be responsible for the double-peaked emission line profiles, however the spatial resolution of the spectrum of the nucleus is not high enough to distinguish between a merger origin or radio jet/cloud interaction origin for the peculiar profiles.

Apart from the radio spectral index anomaly, the radio properties of this source are like a normal FR II source scaled up by a factor of ten, preserving the standard overall

morphology and polarization structure. In the outer regions of the source the magnetic field is likely to be so weak that inverse Compton losses to the Cosmic Microwave Background dominate synchrotron losses.

We are grateful to Mark Whittle for many helpful conversations. We are grateful to Matt Bershady, Randy Phelps, and Mike Siegel for either sharing observing time or taking observations in support of this research. CP acknowledges the support of a Grant-in-aid of Research from Sigma Xi, the Scientific Research Society. This research has made use of the NASA/IPAC Extragalactic Database (NED) which is operated by the Jet Propulsion Laboratory, California Institute of Technology, under contract with the National Aeronautics and Space Administration. We acknowledge the use of NASA's *SkyView* facility (http://skyview.gsfc.nasa.gov) located at NASA Goddard Space Flight Center.

REFERENCES

Abell, G. O. 1958, ApJS, 3, 211

Allington-Smith, J. R., Ellis, R. S., Zirbel, E. L., & Oemler, A., 1993, ApJ, 404, 521

Berkhuijsen, E. M. 1986, A&A, 166, 257

Cardelli, J. A., Clayton, G. C. & Mathis, J. S. 1989, ApJ, 345, 245

Condon, J. J., Cotton, W. D., Greisen, E. W., Yin, Q. F., Perley, R. A., Taylor, G. B., & Broderick, J. J., 1998, AJ, 115, 1693

Cotter, G., Rawlings, S., & Saunders, R. 1996, MNRAS, 281, 1081

Ebeling, H., Edge, A. C., Bohringer, H., Allen, S. W., Crawford, C. S., Fabian, A. C., Voges, W. & Huchra, J. P. 1998, MNRAS, 301, 881

Fabbiano, G., Trinchieri, G., Elvis, M., Miller, L. & Longair, M. 1984, ApJ, 277, 115

Fanaroff, B. L., & Riley, J. M. 1974, MNRAS, 167, 31

Green, P. J., Anderson, S. F. & Ward, M. J. 1992, MNRAS, 254, 30

Halpern, J. P., & Eracleous, M. 1994, ApJ, 433, L17

Heckman, T. M., Smith, E. P., Baum, S. A., van Breugel, W. J. M., Miley, G. K., Illingworth, G. D., Bothun, G. D., & Balick, B., 1986, ApJ, 311, 526

Hill, G. J., & Lilly, S. J., 1991, ApJ367, 1

Kinney, A. L., Calzetti, D. , Bohlin, R. C., McQuade, K. , Storchi-Bergmann, T. & Schmitt, H. R. 1996, ApJ, 467, 38

Lacy, M., Rawlings, S., Saunders, R., & Warner, P. J. 1993, MNRAS, 264, 721

Landolt, A. U., 1992, AJ, 104, 340

Lasker, B. M., Sturch, C. R., McLean, B. J., Russell, J. L., Jenkner, H., & Shara, M. M., 1990, AJ, 99, 2019

Longair, M. S. & Seldner, M. 1979, MNRAS, 189, 433

Miller, N. A., Owen, F. N., Burns, J. O., Ledlow, M. J., & Voges, W. 1999, preprint (astro-ph/9908244)

Monet, D., Bird, A., Canzian, B., Harris, H., Reid, N., Rhodes, A., Sell, S., Ables, H., Dahn, C., Guetter, H., Henden, A., Leggett, S., Levison, H., Luginbuhl, C., Martini, J., Monet, A., Pier, J., Riepe, B., Stone, R., Vrba, F., Walker, R. 1996, USNO-SA1.0, (Washington D.C.: U.S. Naval Observatory)

Mukai, K. 1993, Legacy 3, 21-31

Munn, J. A., Koo, D. C., Kron, R. G., Majewski, S. R., Bershady, M. A., & Smetanka, J. J., 1997, ApJS, 109, 45

Nilsson, K., Valtonen, M. J., Kotilainen, J., & Jaakkola, T., 1993, ApJ, 413, 453

Osterbrock, D. E., 1989, Astrophysics of Gaseous Nebulae and Active Galactic Nuclei, (Mill Valley: University Science Books)

Parma, P., de Ruiter, H., Mack, K.-H., van Breugel, W., Dey, A., Fanti, R., & Klein, U., 1996, A&A, 311, 49

Plucinsky, P. P., Snowden, S. L., Briel, U. G., Hasinger, G., & Pfeffermann, E. 1993, ApJ, 418, 519

Prestage, R. M. & Peacock, J. A. 1988, MNRAS, 230, 131

Rawlings, S., & Saunders, R., 1991, Nature, 349, 138

Rengelink, R. B., Tang, Y., de Bruyn, A. G., Miley, G. K., Bremer, M. N., Röttgering, H. J. A., Bremer, M. A. R. 1997, A&AS, 124,259

Sandage, A. R. 1972, ApJ, 178, 25

Saripalli, L., Gopal-Krishna, Reich, W., & Kühr, H. 1986, A&A, 170, 20

Schlegel, D. J., Finkbeiner, D. P. & Davis, M. 1998, ApJ, 500, 525

Simard-Normandin, M., Kronberg, P. P., & Button, S. 1981, ApJS, 45, 97

Snowden, S. L. 1998, ApJS, 117, 233

Stark, A. A., Gammie, C. F., Wilson, R. W., Bally, J., Linke, R. A., Heiles, C., & Hurwitz, M. 1992, ApJS, 79, 77

Stetson, P. B. 1987, PASP, 99, 191

Strom, R. G. & Willis, A. G. 1980, A&A, 85, 36

Subrahmanyan, R. & Saripalli, L. 1993, MNRAS, 260, 908

Tadhunter, C. N., Morganti, R., Robinson, A., Dickson, R., Villar-Martin, M., & Fosbury, R. A. E. 1998, MNRAS, 298, 1035

Taylor, D., Dyson, J. E., & Axon, D. J. 1992, MNRAS, 255, 351

Valdes, F. 1982, FOCAS User's Manual, (Tucson: NOAO)

Wan, L., & Daly, R. A. 1996, ApJ, 467, 145

Whittle, M. 1989, in Extranuclear Activity in Galaxies, ed. E. Meurs & R. Fosbury (Munich: ESO), 199

Willis, A. G., Strom, R. G., & Wilson, A. S. 1974, *Nature*, 250, 625

Zirbel, E. L. 1996, ApJ, 473, 713

Zirbel, E. L. 1997, ApJ, 476, 489

Zirbel, E. L., & Baum, S. A. 1995, ApJ, 448, 521

Zwicky, F., Herzog, E., Wild, P., Karpowicz, M., & Kowal, C. 1961-68, Catalogue of Galaxies and Clusters of Galaxies, (Pasadena: CIT)

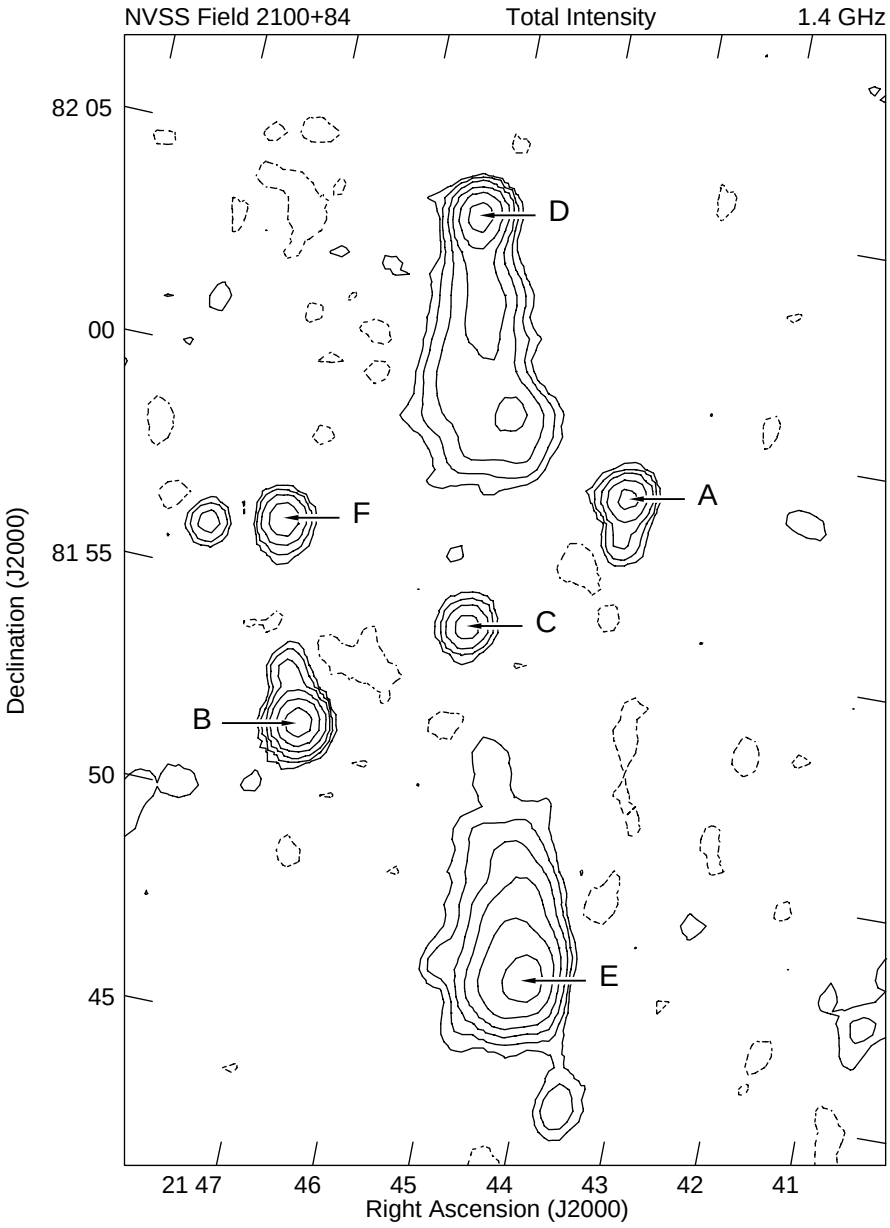

Fig. 1.— Contour plot of the NVSS 1.4 GHz total intensity data for the field. Contours are shown at -1, 1, 2,4, 8, 16, and 32 mJy per CLEAN beam area.

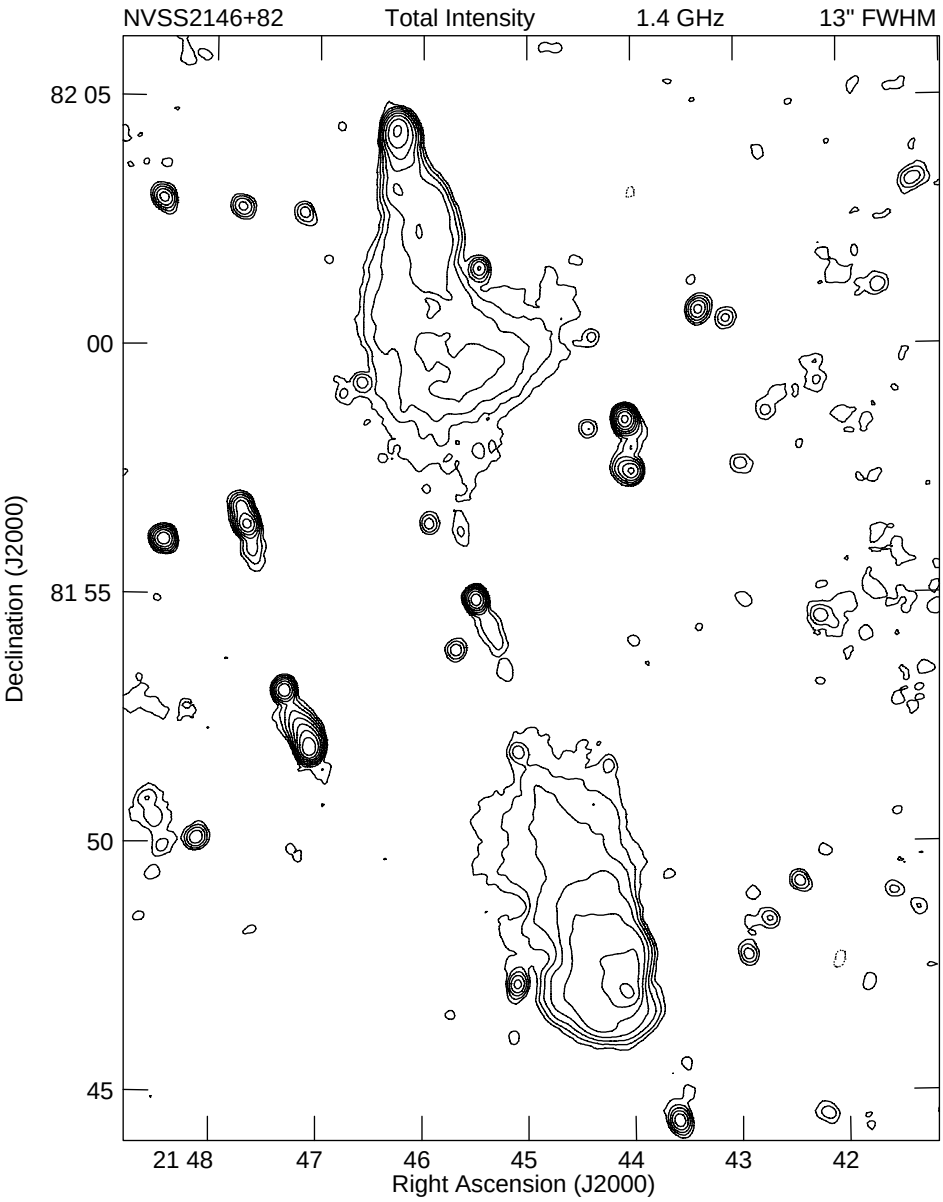

Fig. 2.— Contour plot of the new 1.4 GHz total intensity data for the field at 13″ (FWHM) resolution. Contours are shown at -1, 1, 2,4, 8, 16, 32 and 64 times 100 μJy per CLEAN beam area.

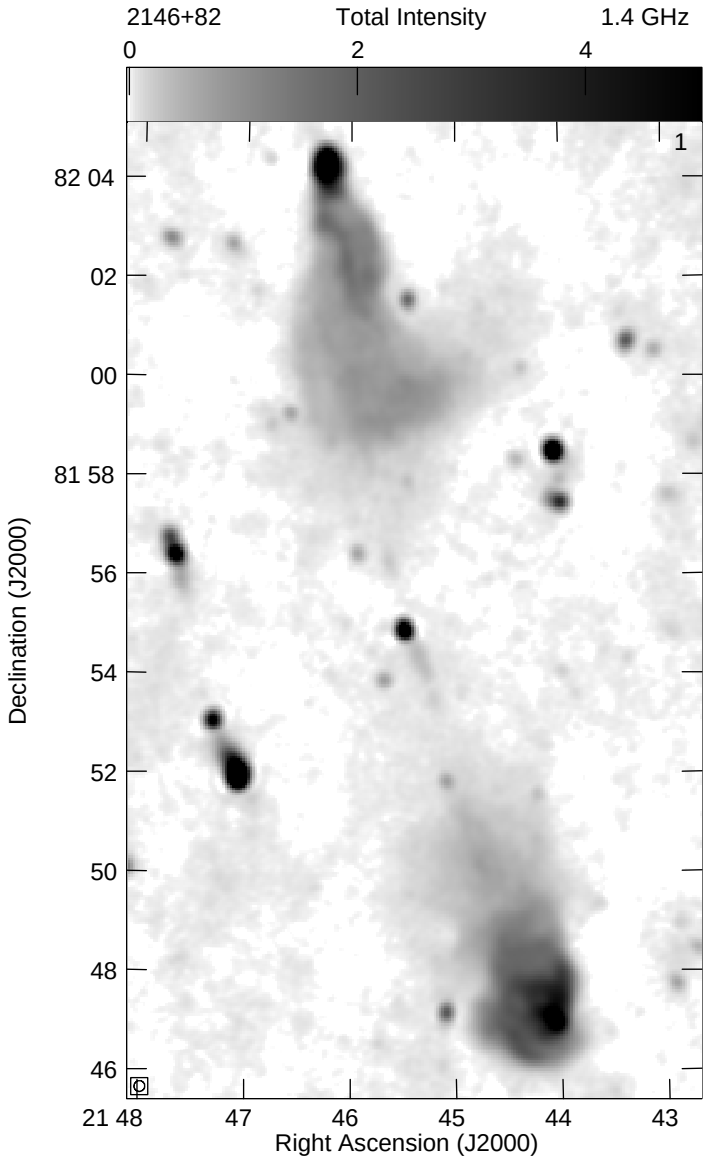

Fig. 3.— Gray scale image at 13″ (FWHM) resolution using a nonlinear transfer function to emphasize the lower brightness levels. The jet and strong filaments in the lobes can be seen.

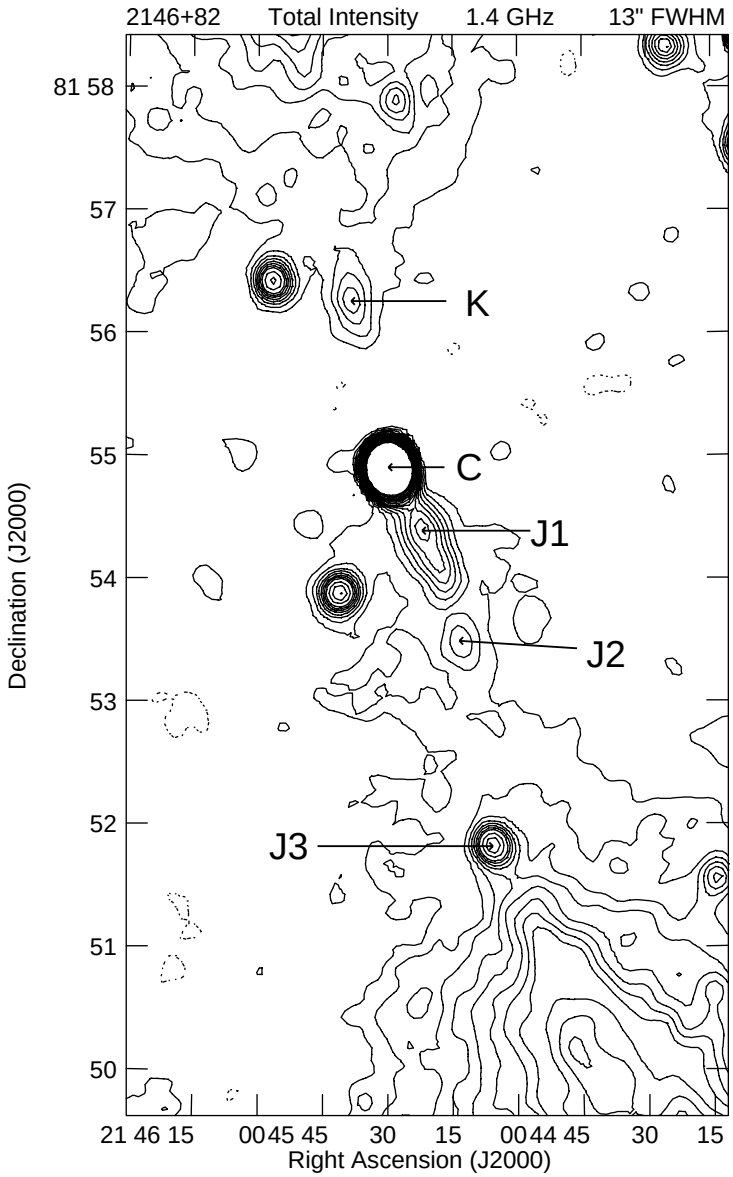

Fig. 4.— Contour plot of the new 1.4 GHz total intensity data for the field at 13″ (FWHM) resolution. Contours are shown at -1, 1, 2, 3, 4, 5, 6, 7, 8, 10, and 12 times 50 μJy per CLEAN beam area. The core and various features in the jet are marked.

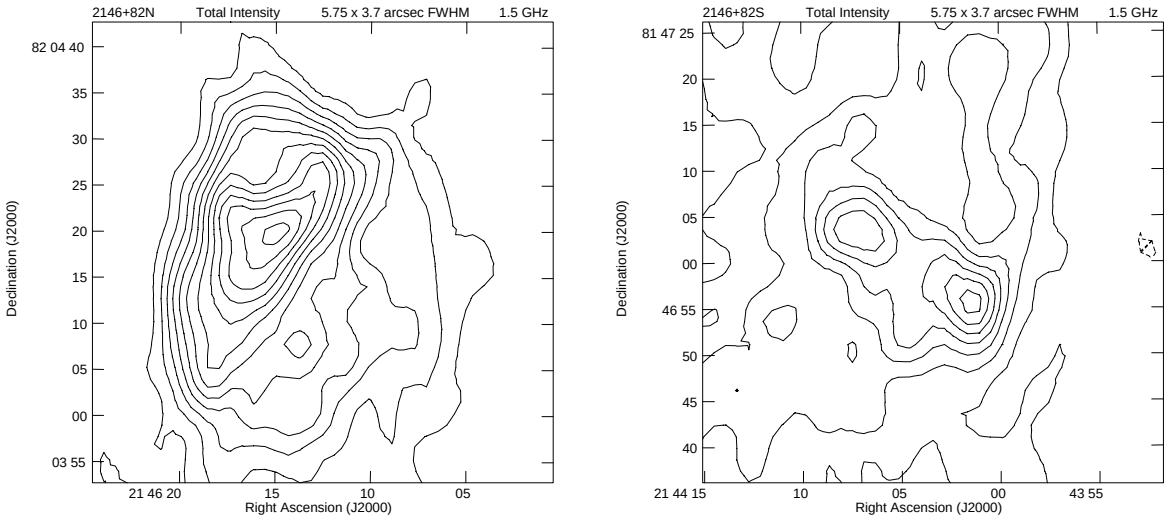

Fig. 5.— Contour plot of the 1.5 GHz total intensity data from the B configuration over the north D (left) and south E (right) hot spots of the source at $5\overset{''}{.}75$ by $3\overset{''}{.}7$ (FWHM) resolution. Contours are shown at a linear interval of 0.25 mJy per CLEAN beam area

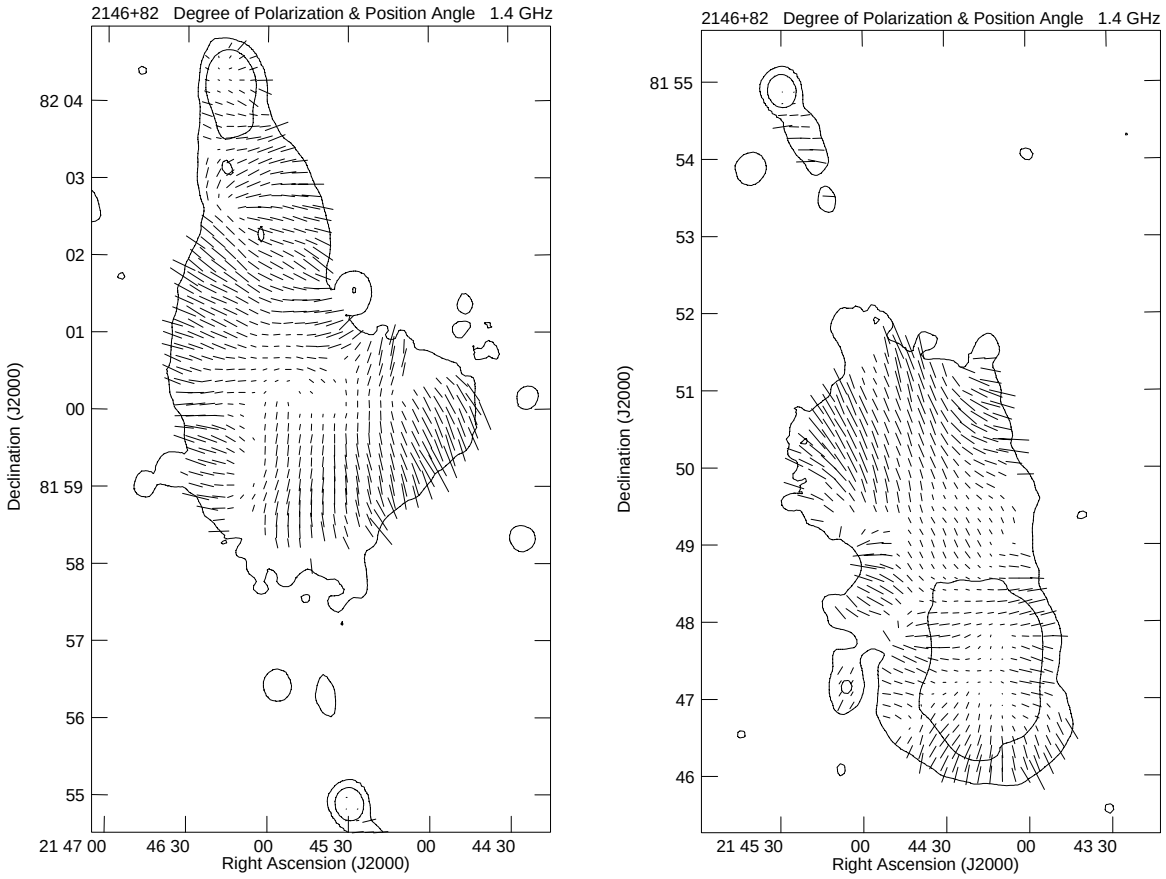

Fig. 6.— Distribution of degree of 1.4 GHz linear polarization p and **E**-vector position angle χ over the north D (left) and south E (right) lobes of the source at $13''$ (FWHM) resolution, superposed on selected contours of total intensity. A vector of length $15''$ corresponds to p=0.5.

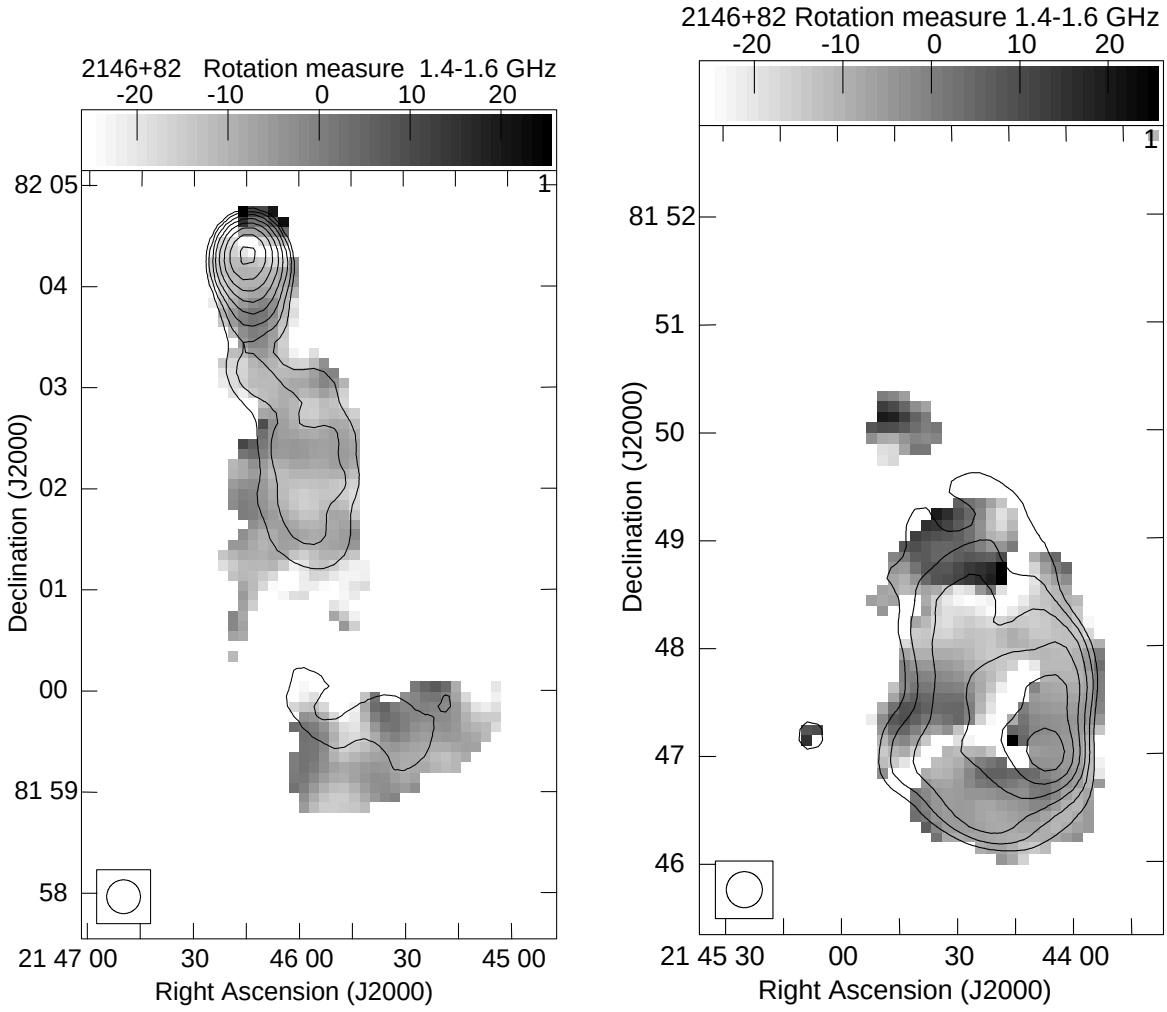

Fig. 7.— Gray scale representation of the rotation measure at $20''$ resolution with superimposed contours of the 1.6 GHz total intensity at the same resolution. The bar at the top gives the grayscale values and the resolution is shown in the lower–left corner. The north lobe is shown in the left and the south lobe on the right.

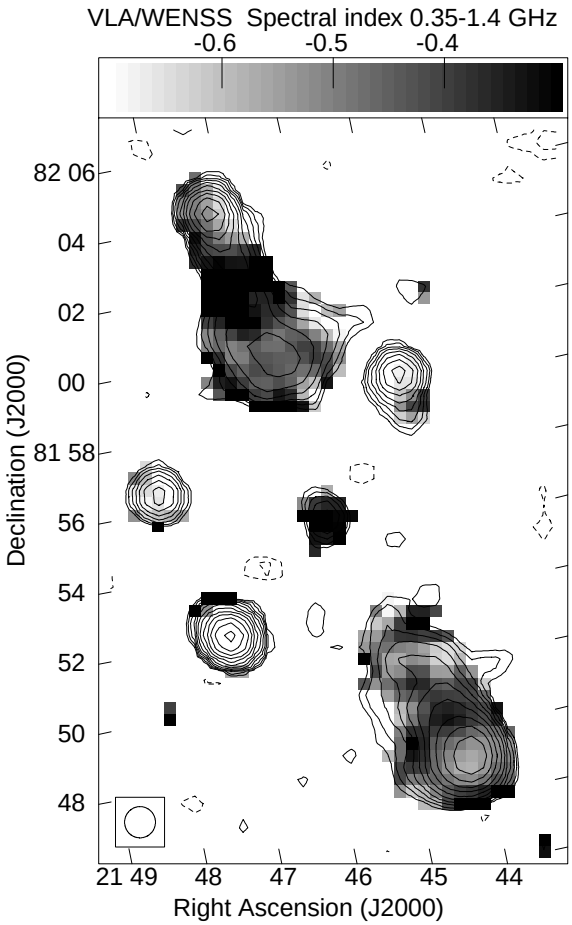

Fig. 8.— Gray scale representation of the spectral index distribution derived from VLA measurements at 1.4 GHz and the 0.35 GHz WENSS image with superimposed contours from the VLA image. The resolution is $54''$ (FWHM), illustrated in the lower–left and the bar at the top gives the gray scale values.

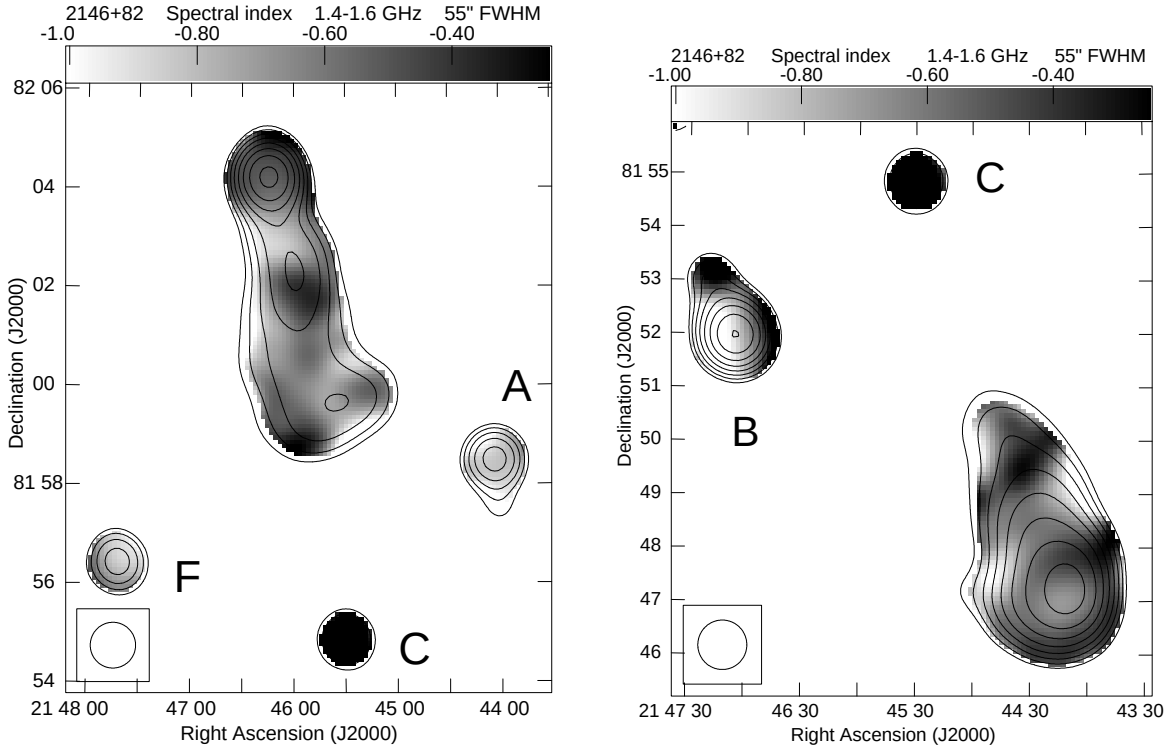

Fig. 9.— Gray scale representation of the spectral index at 55″ resolution derived from the 1.36 and 1.63 GHz data with superimposed contours of the 1.63 GHz total intensity at the same resolution. The bar at the top gives the gray scale values and the resolution is shown in the lower–left corner. The north lobe is shown in the left and the south lobe on the right.

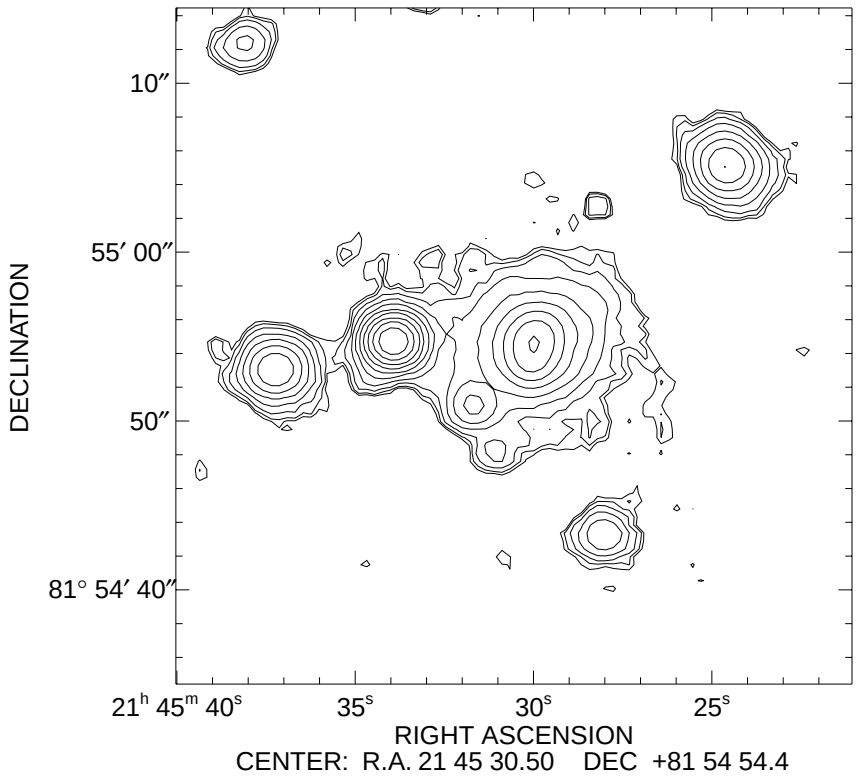

Fig. 10.— A contour plot of the V band surface brightness of the region immediately surrounding the host galaxy of NVSS 2146+82. The object just east of the host galaxy (at center) is a foreground star. The remaining four discrete objects all have non-stellar PSFs, indicating that they are very likely galaxies. The object to the northwest of NVSS 2146+82 is a galaxy and has a spectroscopic redshift from our WIYN program of $z = 0.144$.

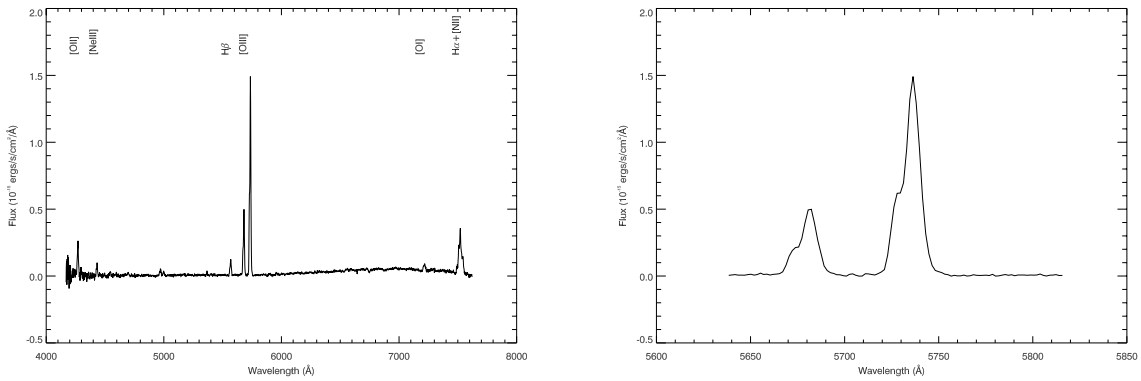

Fig. 11.— Spectrum of the host galaxy of NVSS 2146+82. The left panel shows the full spectrum, with several of the stronger emission features identified in Table 4 are marked. Most of the emission lines have a double-peaked profile, as illustrated in the right panel with the [O III] $\lambda\lambda$4959, 5007 pair.

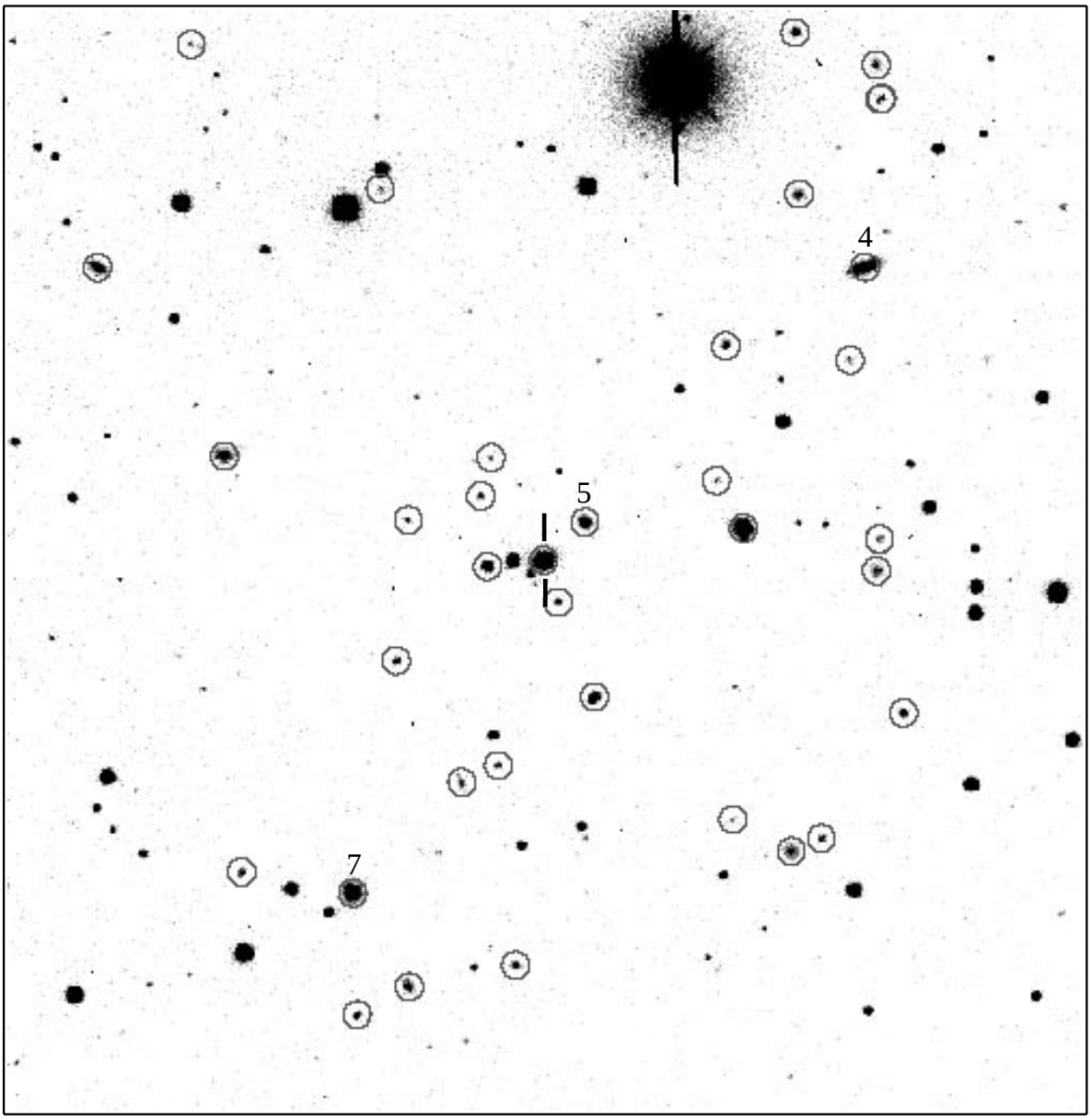

Fig. 12.— A view of the field surrounding NVSS 2146+82 from the central region of our KPNO 4 meter image (north is up, east to the left). This field is 0.5 Mpc on a side at the redshift of NVSS 2146+82, and it contains 34 objects down to $m_v = 21.3$ ($M_V \geq -19$ at $z = 0.145$) that are morphologically identified as galaxies. For reference, the host galaxy of NVSS 2146+82 is marked with hash marks, and the three galaxies in this region that we measured spectroscopic redshifts for are marked with their ID numbers from Table 5

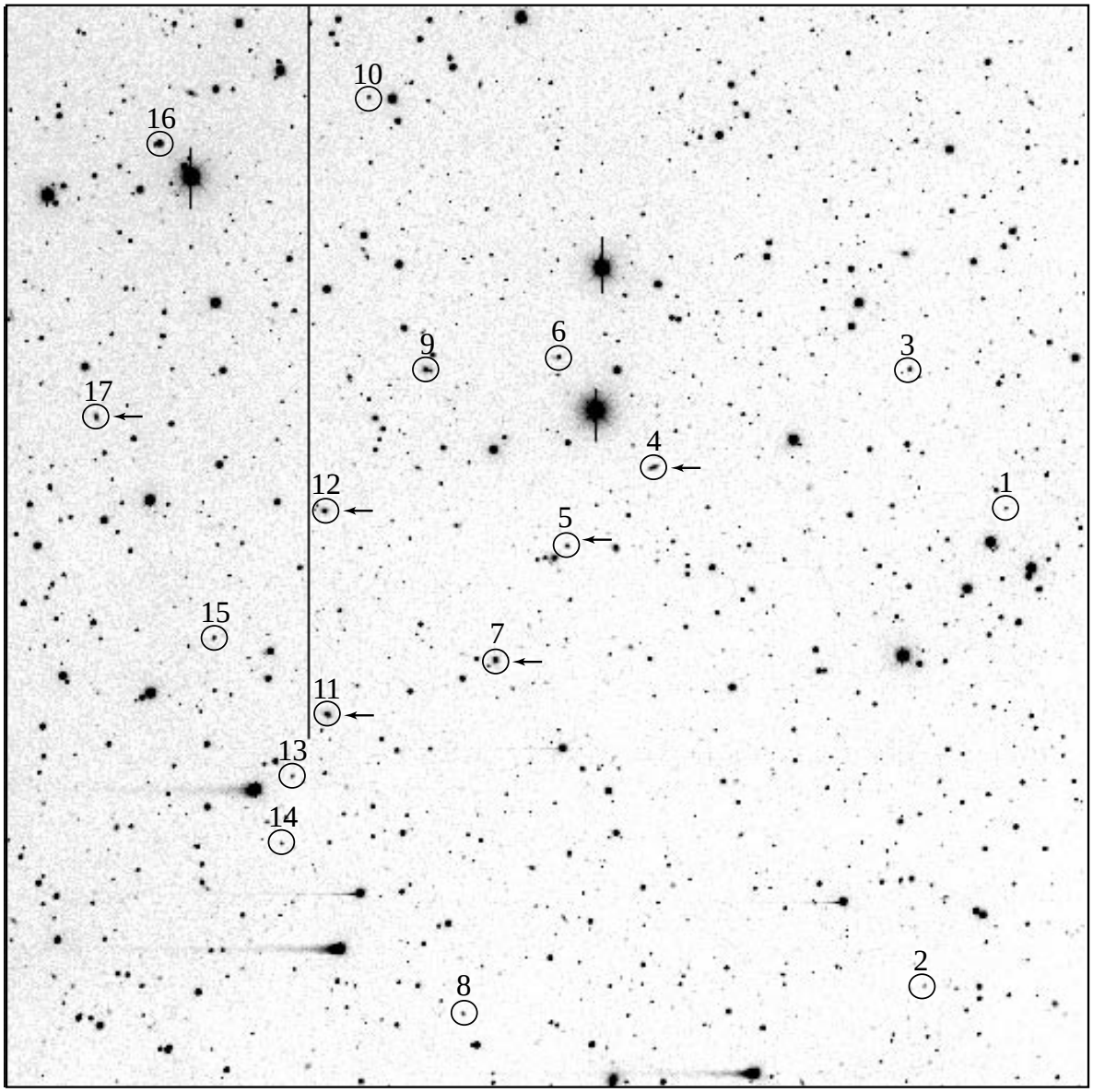

Fig. 13.— The full field that we observed with the KPNO 4 meter surrounding NVSS 2146+82. In this image, the 17 galaxies with spectroscopic redshifts are circled and identified with their ID number from Table 5. Those objects with reliable redshifts in the range $0.135 < z < 0.149$ are marked with arrows. NVSS 2146+82 is the galaxy just outside of the southeast edge of the circle surrounding galaxy 5.

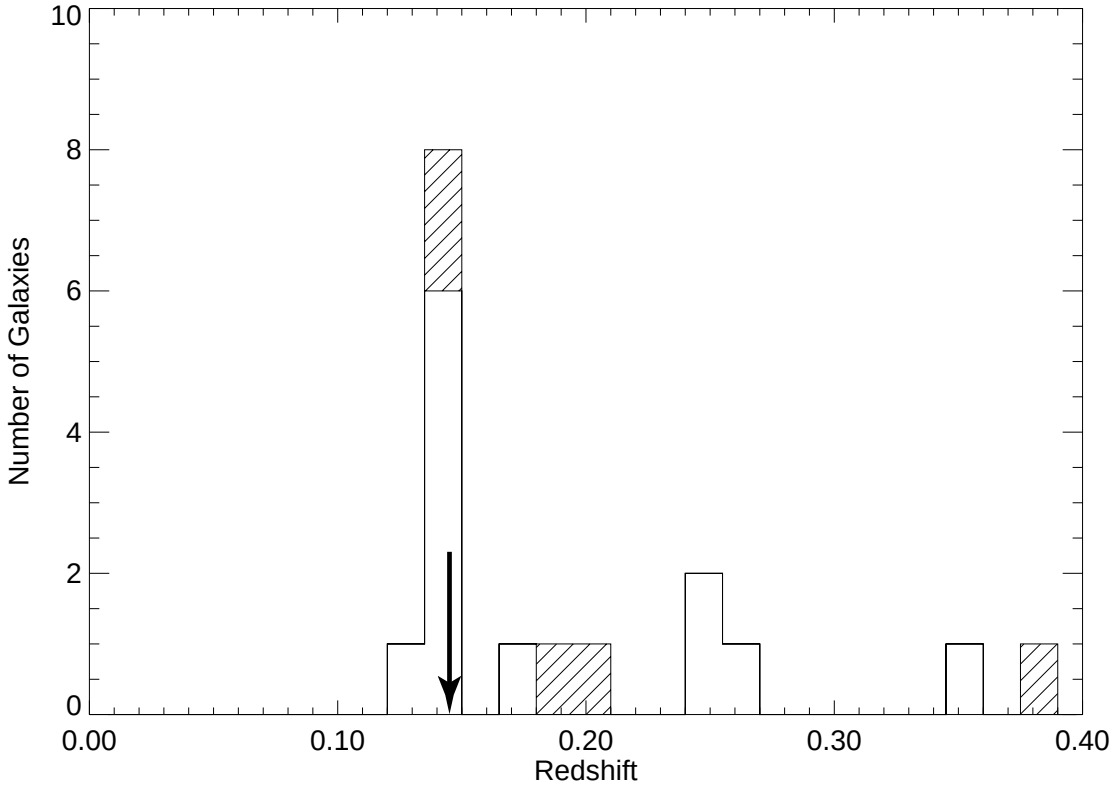

Fig. 14.— A histogram of the redshifts of the 17 galaxies that we obtained spectra for with the WIYN. The empty histogram is the distribution of redshifts that have $q > 3$, and the hatched histogram is the distribution of the lower quality redshifts. The arrow shows the redshift for NVSS 2146+82, $z = 0.145$. The peak in this diagram is centered around $z = 0.1425$, showing that 6 – 8 galaxies in our sample of 17 share the same redshift as NVSS 2146+82.

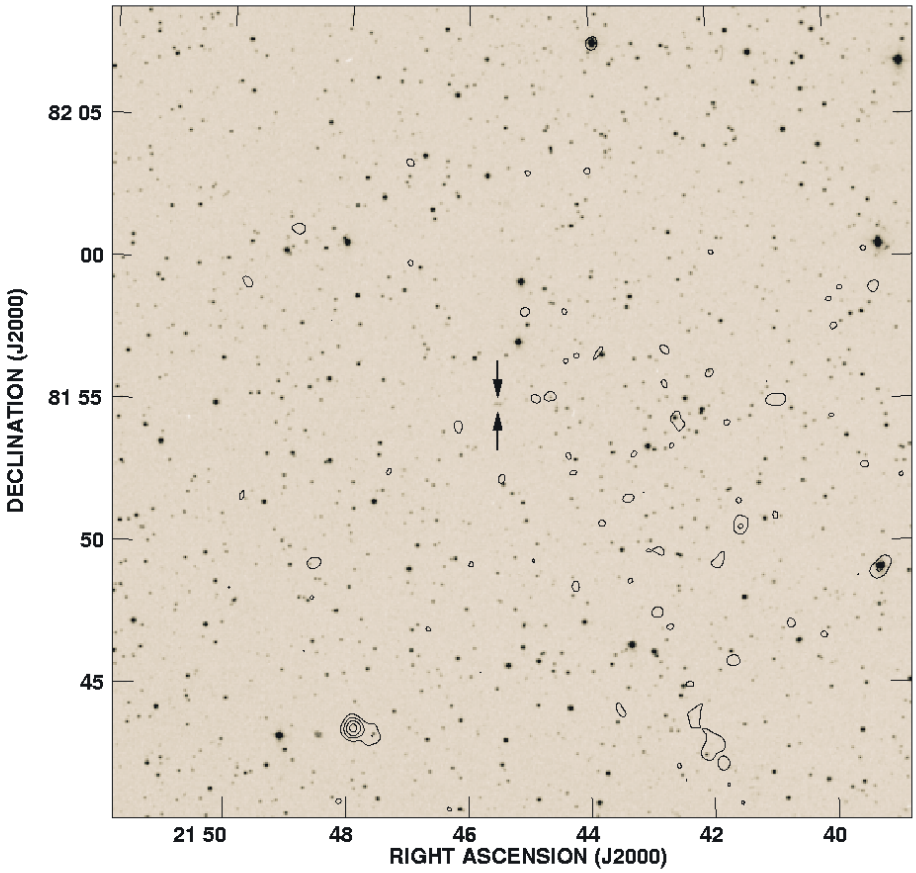

Fig. 15.— A contour plot of the *ROSAT* HRI X-ray image in the 0.5–2.0 keV band. The X-ray image has been corrected for non-X-ray background, vignetting, and exposure and convolved with a 2 arcsec sigma gaussian beam. The contours are superposed on an optical image from the Digitized Sky Survey (Lasker et al. 1990). The base contour level is 1.1 counts/pixel. The contours plotted are multiples (1, $2^{1/2}$, 2^{1}, $2^{3/2}$, ...) of the base contour level. The arrows indicate the position of the host galaxy.

Table 1: VLA Observing Log

VLA Configuration	Observing Date	Center Frequencies (MHz)	Bandwidth (MHz)	Number of Fields	Integration (min)
A	1995 Jul 08	8415, 8465	50	6	5
A	1995 Jul 08	4835, 4885	50	6	6
B	1995 Dec 23	1365, 1636	12.5	3	13
C	1996 Feb 15	1365, 1636	25	3	22
D	1996 Sep 02	1365, 1636	25	3	18
B	1995 Dec 23	327.5, 333	3.1	1	69
C	1996 Feb 15	327.5, 333	3.1	1	30
D	1996 Sep 02	327.5, 333	3.1	1	7.5
BnC	1997 Jun 17	1365, 1435	50	3	185

Table 2: Flux Densities

	0.35 GHz[a]	1.4 GHz	4.9 GHz	8.4 GHz	$\alpha_{0.35}^{1.4}$
Total	0.99 ± 0.02 Jy	0.53 ± 0.1 Jy			-0.45 ± 0.06
N lobe	0.43 ± 0.01 Jy	0.24 ± 0.05 Jy			-0.42 ± 0.07
S lobe	0.52 ± 0.01 Jy	0.27 ± 0.05 Jy			-0.47 ± 0.06
C	23 ± 2 mJy	13.6 ± 0.5 mJy	6.8 ± 0.2 mJy	3.4 ± 0.2 mJy	-0.38 ± 0.03
J1		1.3 ± 0.2 mJy			
J2		0.3 ± 0.2 mJy			
J3		0.8 ± 0.2 mJy			
K		0.7 ± 0.2 mJy			

[a] 0.35 GHz measurements are from the WENSS image.

Table 3: Mean Aperture Magnitudes for NVSS 2146+82 Host Galaxy

Night	Filter	Magnitude	Error
2	U	19.57	0.45
1	B	18.83	0.09
1	V	17.53	0.04
2	R	17.19	0.07
2	I	16.47	0.07

Table 4: Emission Line Data for NVSS 2146+82

Species	$\lambda_{\rm red}$ Å	$z_{\rm red}$	$\lambda_{\rm blue}$ Å	$z_{\rm blue}$	Flux[a] 10^{-15} erg/sec/cm^2	Luminosity[a] 10^{41} erg/sec h_{50}^{-2}
[O II] λ3727	4262.5	0.1436	4269.6	0.1455	7.4±0.5	7.6±0.5
[Ne III] λ3869	4425.3	0.1439	4432.6	0.1458	2.8±0.3	2.9±0.3
[Ne III] λ3967[b]			4545.1	0.1456	0.9±0.1	0.9±0.1
Hδ	4693.7	0.1443	4698.2	0.1454	0.3±0.1	0.3±0.1
Hγ	4963.9	0.1436	4971.9	0.1455	1.4±0.2	1.4±0.2
[O III] λ4363[b]			4998.8	0.1457	0.8±0.1	0.8±0.1
He II λ4686	5360.8	0.1440	5367.5	0.1454	0.8±0.2	0.8±0.2
Hβ	5560.5	0.1438	5569.2	0.1456	3.0±0.4	3.1±0.4
[O III] λ4959	5672.4	0.1439	5681.6	0.1457	12.3±1.1	12.7±1.1
[O III] λ5007	5727.2	0.1439	5736.4	0.1457	35.7±3.2	36.9±3.3
[O I] λ6300	7206.2	0.1438	7217.4	0.1456	1.6±0.4	1.7±0.4
[N II] λ6548	7493.7	0.1444	7505.4	0.1462	1.7±0.3	1.8±0.3
Hα	7508.9	0.1442	7520.3	0.1459	8.9±1.0	9.2±1.0
[N II] λ6584	7530.6	0.1438	7542.8	0.1457	5.1±0.6	5.3±0.6

[a] These values have been dereddened using a value of $A_V = 0.9$. Errors include only calibration and measurement error, error in reddening is not included.

[b] These lines were not resolved into a blue and red component; the values listed in the table were determined by fitting the profile with a single gaussian.

Table 5: Redshifts of Candidate Cluster Members in the Field of NVSS 2146+82

Galaxy ID	$\alpha_{2000.0}$	$\delta_{2000.0}$	z	q	m_v
1	21:42:18.5	81:55:34	0.242	5	20.0
2	21:42:56.3	81:48:29	0.378	3	20.2
3	21:42:58.5	81:57:40	0.350	5	19.4
4	21:44:47.8	81:56:15	0.145	6	18.8
5	21:45:24.5	81:55:05	0.144	6	19.3
6	21:45:27.7	81:57:54	0.267	6	19.4
7	21:45:54.8	81:53:23	0.135	6	18.4
8	21:46:08.8	81:48:08	0.123	6	20.1
9	21:46:24.3	81:57:43	0.243	6	18.4
10	21:46:48.6	82:01:46	0.183	2	19.8
11	21:47:05.7	81:52:35	0.144	6	18.3
12	21:47:07.2	81:55:36	0.145	6	18.4
13	21:47:20.4	81:51:40	0.149	1	19.7
14	21:47:24.7	81:50:40	0.173	6	20.0
15	21:47:53.7	81:53:43	0.208	2	19.4
16	21:48:19.9	82:01:03	0.143	1	17.7
17	21:48:44.3	81:56:59	0.148	6	18.9

Table 6: Giant Radio Galaxies

IAU Name	Other Name	z	LAS (arcsec)	$\log P_{1.4}$ (h_{50}^{-2} W Hz^{-1})	LLS (h_{50}^{-1} Mpc)
1003+351	3C 236	0.0989	2478	26.37	6.04
2146+82	**NVSS 2146+82**	**0.1450**	**1175**	**25.69**	**3.91**
0821+695	8C 0821+695	0.5380	402	26.30	2.94
1637+826	NGC 6251	0.0230	4500	24.73	2.89
0319-454		0.0633	1644	25.83	2.72
1549+202	3C 326	0.0885	1206	26.08	2.67
1358+305	B2 1358+305	0.2060	612	25.93	2.64
1029+570	HB 13	0.0450	2100	24.57	2.54
0503-286		0.0380	2400	25.23	2.48
1452-517	MRC 1452-517	0.08	1218	25.66	2.48
0114-476	PKS 0114-476	0.1460	702	26.51	2.36
1127-130	PKS 1127-130	0.6337	297	27.53	2.30
0707-359	PKS 0707-359	0.2182	492	26.71	2.21
1910-800		0.3460	366	26.65	2.18
0745+560	DA 240	0.0350	2164	25.39	2.07
0313+683	WENSS 0313+683	0.0902	894	25.64	2.01